Bifurcation instability of substrate-supported metal films under biaxial in-plane tension

Zheng Jia [a],*, Teng Li [b],*

[a] *Department of Engineering Mechanics, Key Laboratory of Soft Machines and Smart Devices of Zhejiang Province, Zhejiang University, Hangzhou, 310027, China*
[b] *Department of Mechanical Engineering, University of Maryland, College Park, MD 20742, USA*

A B S T R A C T

The stretchability of metal materials is often limited by the onset and development of necking instability. For instance, necking of lithium metal often occurs at low strains and thus hinders its practical applications in stretchable lithium batteries. Substrate/metal bilayers are emerging as a promising solution to the stringent stretchability requirement of metal electrodes and current collectors in flexible and stretchable batteries. So far, a comprehensive understanding of the bifurcation instability of substrate-supported metal layers under arbitrary biaxial in-plane tensile loading still remains elusive. Most existing theoretical and numerical studies of the bifurcation instability of substrate-supported metal layers assume either plane strain condition or single-necking mode (i.e., a single diffusive neck occurs). However, in conducted experiments, substrate/metal bilayers are subjected to uniaxial tensile loading and formation of multiple necks is observed during the tests. This paper presents an all-wavelength bifurcation analysis to understand the deformation instability of substrate/metal bilayers under arbitrary biaxial tensile loadings, from equibiaxial tension, to plane-strain tension, and to uniaxial tension. Two representative bilayer structures are investigated, namely, a metal layer supported by a plastic substrate and a metal layer supported by an elastomer substrate. The analysis predicts three bifurcation modes of substrate/metal bilayers, including single-necking mode, multiple-necking mode, and surface mode. The results quantitatively demonstrate the bifurcation retardation effect of the supporting substrate: the stiffer/thicker is the substrate, the higher is the bifurcation limit. More importantly, it is further shown that there exists a theoretical upper bound of the bifurcation limit of a substrate/metal bilayer structure, which has not been reported before. Understandings from the present study may shed light on the optimal design of substrate/metal bilayer structures with enhanced deformability under complex biaxial loading conditions.

© 2019 Elsevier Ltd. All rights reserved.

1. Introduction

The past decade has witnessed a surge of interest in flexible and stretchable electronics, an emerging technology with an array of promising applications, such as epidermal electronics (Kim et al., 2011; Yang et al., 2015), wearable devices (Son et al., 2014) and bio-inspired electronic eyes (Song et al., 2013). To power these devices, stretchable batteries, especially

lithium-based batteries of high specific capacity, with comparable stretchability to the stretchable devices are highly desired (Fu et al., 2016; Liu et al., 2017; Xu et al., 2013; Zhang et al., 2015). Flexible batteries are often subject to large and repeated deformation to adapt to the dynamic shape change of stretchable electronic devices in use. The functional components of flexible batteries, such as metal current collectors and electrodes, need to sustain cyclic deformation at a strain level up to tens of percent. However, metal current collectors such as aluminum and copper used in batteries rupture when stretched beyond 1%–2% of tensile strain (Huang and Spaepen, 2000; Nicola et al., 2006). Necking of lithium metal anodes in lithium batteries occurs at a strain of 25%, followed by a ductile fracture (Gorgas et al., 1981; Liu et al., 2018). The need for enhancing the stretchability of metal materials to meet the stringent requirement of stretchable batteries and electronics has induced an impetus to develop more advanced structural elements and functional components such as substrate-supported metal layers (Lacour et al., 2003; Liu et al., 2018; Vandeparre et al., 2013). Indeed, substrate-supported lithium metal anodes have been proven to exhibit stable mechanical and electrochemical performance (Liu et al., 2018). However, fundamental mechanism underpinning the enhanced stretchability of substrate-supported metal films under complex loading conditions remains elusive.

Stretchability of freestanding metal layers under in-plane loading is often limited by the initiation and development of strain localization, i.e., necking instability (Franz et al., 2013; Hutchinson and Neale, 1978; Storen and Rice, 1975; Zhang and Wang, 2012). A freestanding metal layer deforms uniformly under a modest in-plane tensile loading. The uniform deformation of the metal layer becomes unstable when the loading increases to a sufficiently high level: infinitesimal perturbation of the metal layer, such as non-uniform thickness or pre-existing defects, starts to grow in amplitude, leading to local thinning in certain locations of the metal layer. On one hand, localized deformation due to local thinning leads to increased stress level at the necking location (i.e., geometric softening); on the other hand, the metal material at the site of necking hardens under plastic deformation to sustain the increased stress level (i.e., material hardening). When the geometric softening prevails over material hardening, the onset of necking instability occurs: the local thinning of metal layer continues on to form a single neck, rupturing the metal film. Since a freestanding metal film fails by a single neck, the rupture strain of a freestanding metal film is also named as the necking limit. By volume conservation, at the site of rupture, the local thinning causes a local elongation on the order of the film thickness. Given the small thickness-to-length ratio of the film, this local elongation contributes little to the overall rupture strain. As a result, freestanding metal films usually have small rupture strains (Espinosa et al., 2003; Li et al., 2005; Li and Suo, 2006). There exist a large amount of studies on the experimental and numerical determination of necking limits for freestanding metal films with different material behaviors such as plastic anisotropy (Kuroda and Tvergaard, 2000; Zhang and Wang, 2012), strain-rate sensitivity (Ghosh, 1977; Khan and Baig, 2011; Zhang and Ravi-Chandar, 2006), kinematic hardening (Bettaieb and Abed-Meraim, 2017; Tvergaard, 1978), and damage-induced softening (Haddag et al., 2009; Mansouri et al., 2014). However, localized necking limits the maximum allowable strain that a freestanding metal film can undergo during the operation of stretchable electronic devices. Therefore, the development of new strategies to retard the occurrence of necking formation is of significant practical interest in the field of stretchable batteries and electronics.

As abovementioned, the local elongation due to necking formation requires space to accommodate. This space is available to the freestanding film as the ruptured halves can freely move apart, but is unavailable to the film bonded to a substrate subject to a modest tensile strain since the substrate constrains the deformation of metal layers. Consequently, a plastic or an elastomer substrate may delocalize the strain field in the metal film, carrying the film to the strain far beyond the rupture strain of a freestanding film (Li et al., 2005). Guided by this principle, in the field of modern technologies, and especially stretchable batteries, improving the stretchability of metal materials is achieved by bonding deformable substrates (e.g., elastomer or plastic) to metal layers. The large rupture strains of metal films bonded to plastic or elastomer substrates have been demonstrated in experiments (Gruber et al., 2004; Lu et al., 2007; Xiang et al., 2005), theoretical analysis and finite element simulations (Bigoni et al., 1997; Jia and Li, 2013; Li et al., 2005; Xue and Hutchinson, 2007). For example, plastic-supported thin metal films can sustain tensile strains up to 50% before rupture (Alaca et al., 2002; Hommel and Kraft, 2001; Lu et al., 2007, 2010; Yu and Spaepen, 2004). Additionally, plastic/elastomer-supported metal layers have been proven to show significantly improved ductility and enhanced energy absorption when subject to high-intensity impulsive loads (Ben Bettaieb and Abed-Meraim, 2015; Jia and Li, 2013; Xue and Hutchinson, 2007). It is also demonstrated in experiments and simulations that the substrate constraint to the necking development in the metal film disappears when the metal layer detaches from the substrate (Li et al., 2005; Lu et al., 2007). When substrate-supported metal films are subject to dynamic stretching, the inertia effect on necking retardation and necking modes has also been investigated (Amini and Nemat-Nasser, 2010; Amini et al., 2010; Morales et al., 2011; Shenoy and Freund, 1999; Xue and Hutchinson, 2008).

Despite the success in effectively enhancing the rupture strain of metal films; an in-depth theoretical understanding of the bifurcation instability of substrate-supported metal layers under biaxial in-plane tension is still far from being complete. It is worth noting that freestanding metal films fail by a single neck, which is captured by the bifurcation analysis at the long-wavelength limit (i.e., wavelength of the necking pattern is infinitely large). In stark contrast, experiments (Lu et al., 2007; Xiang et al., 2005) and simulations (Li and Suo, 2007) have revealed that substrate-supported metal film under in-plane biaxial tension may fail by forming multiple necks (a necking pattern at an intermediate wavelength) or surface instability (non-uniform deformation at very short wavelength, i.e., the short-wavelength limit). This could be attributed to the strain-delocalization effect of the substrate. Since most existing theoretical/numerical studies only consider the bifurcation of substrate-supported metal films at the long-wavelength limit (Ben Bettaieb and Abed-Meraim, 2015; Bettaieb and Abed-Meraim, 2017; Jia and Li, 2013; Xue and Hutchinson, 2007, 2008), an all-wavelength bifurcation analysis is needed

to understand the deformation instability of substrate-supported metal films. Moreover, substrate-supported metal layers in stretchable electronic devices are often subject to large and complicated in-plane biaxial tensile loading. For example, the epidermal electronics covering the human skin experiences large biaxial stretches (Kim et al., 2011). However, most existing theoretical/numerical studies assume plane-strain condition in the bifurcation analysis of bilayer structure (Guduru et al., 2006; Guduru and Freund, 2002; Shenoy and Freund, 1999). Consequently, theoretical understanding of the bifurcation instability of substrate/metal bilayer under arbitrary biaxial in-plane tension remains elusive so far and requires further investigation.

Hutchinson and Tvergaard conducted bifurcation analysis to investigate the bifurcation instability of a freestanding metal film under arbitrary biaxial in-plane tension (Hutchinson and Tvergaard, 1980). In this study, we extend their effort to substrate-supported metal films (i.e., a metal film bonded to the substrate via a perfect interface without delamination) under arbitrary biaxial in-plane tension. Two representative bilayer structures are studied, namely, a metal layer supported by a stiff plastic substrate, and a metal layer supported by a compliant elastomer substrate, respectively. We report quantitative correlations between bifurcation limit, bifurcation modes and design parameters (material properties and substrate/film thickness) of substrate-supported metal films in the full range of biaxial in-plane tension. Most importantly, we show that there exists a theoretical upper bound of the bifurcation limit of a substrate/metal bilayer structure and offer insights on the underlying physics, which has not been reported previously. The rest of the paper is organized as follows. Section 2 describes the constitutive equations and bifurcation analysis procedure for investigating the bifurcation limit of substrate-supported metal films. Section 3 reports numerical results of the bifurcation limit of substrate/film bilayers. Effect of substrate on the bifurcation limit and bifurcation mode is discussed. Conclusions and remarks are given in Section 4.

2. Mechanics model

2.1. Constitutive relations

We describe the constitutive law of both the metal layer and the elastomer layer using the finite strain J2 deformation theory of plasticity developed by Biot, Hutchinson, and Tvergaard (Biot, 1965; Hutchinson and Tvergaard, 1980), as recapped below. The materials are considered to be rate-independent and incompressible, with the constitutive law of the form

$$\bar{\sigma}_{ij} = L_{ijkl}\dot{\varepsilon}_{kl} + \dot{p}\delta_{ij} \tag{1}$$

Here, $\bar{\sigma}_{ij}$ is the Jaumann rate of the Cauchy stress, L_{ijkl} is the instantaneous moduli, $\dot{\varepsilon}_{kl}$ is the Eulerian strain rate, $\dot{p}$ is the hydrostatic stress rate, δ_{ij} is the Kronecker delta. (Hereinafter, $^-$ denotes objective Jaumann rates, while $^{\cdot}$ denotes time rates). The instantaneous moduli L_{ijkl} is given as

$$L_{ijkl} = \frac{2}{3}E_s\left[\frac{1}{2}\left(\delta_{ik}\delta_{jl} + \delta_{il}\delta_{jk}\right) - \frac{1}{3}\delta_{ij}\delta_{kl}\right] - \frac{(E_s - E_t)s_{ij}s_{kl}}{\sigma_e^2} + Q_{ijkl} \tag{2}$$

where s_{ij} is the deviatoric stress and $\sigma_e = \sqrt{\frac{3}{2}s_{ij}s_{ij}}$ is the effective stress, E_s and E_t are the secant modulus and tangent modulus of the uniaxial true stress-strain curve at σ_e, respectively. The last term Q_{ijkl} satisfies the indicial symmetry that $Q_{ijkl} = Q_{jikl} = Q_{ijlk} = Q_{klij}$ and only the following components are non-trivial in principal axes.

$$Q_{1212} = \frac{1}{3}E_s[(\varepsilon_1 - \varepsilon_2)\coth(\varepsilon_1 - \varepsilon_2) - 1] \tag{3.1}$$

$$Q_{1313} = \frac{1}{3}E_s[(\varepsilon_1 - \varepsilon_3)\coth(\varepsilon_1 - \varepsilon_3) - 1] \tag{3.2}$$

$$Q_{2323} = \frac{1}{3}E_s[(\varepsilon_2 - \varepsilon_3)\coth(\varepsilon_2 - \varepsilon_3) - 1] \tag{3.3}$$

Combining Eqs. (2) and (3.1)–(3.3), we can prove that instantaneous moduli L_{ijkl} for the metal layer share the indicial symmetry that

$$L_{ijkl} = L_{jikl} = L_{ijlk} = L_{klij} \tag{4}$$

Explicit expressions of instantaneous moduli L_{ijkl} are given in Appendix A1.

Consider a flat film under in-plane biaxial loading. Without loss in generality, the film is presumed to be in the plane prescribed by axes x_2 and x_3, with the axis x_1 being perpendicular to the film. For an in-plane biaxial proportional straining history, the strain components are specified by

$$\varepsilon_2 = X \cos\alpha \tag{5.1}$$

$$\varepsilon_3 = X \sin\alpha \tag{5.2}$$

$$\varepsilon_1 = -\varepsilon_2 - \varepsilon_3 \tag{5.3}$$

For proportional straining, α is fixed and X is monotonically increased. Since $\tan\alpha$ prescribes the strain ratio $\varepsilon_3/\varepsilon_2$, α can be defined as the strain ratio angle. Three representative in-plane tensile loading conditions are identified by the value of α: (i) $\alpha = 45°$ for equibiaxial tension with $\varepsilon_2/\varepsilon_3 = 1$, (ii) $\alpha = 90°$ for plane-strain tension with $\varepsilon_2/\varepsilon_3 = 0$, and (iii) $\alpha = 116.6°$ for uniaxial tension along the x_3 direction with $\varepsilon_2/\varepsilon_3 = -0.5$. Moreover, for $45° \le \alpha \le 116.6°$, ε_3 is always greater than ε_2. The J2 deformation theory gives the relation between the principal strain and the principal deviatoric stress as $\varepsilon_i = \frac{3}{2E_s}s_i = \frac{3\varepsilon_e}{2\sigma_e}s_i$. Imposing the biaxial proportional straining history to the structure, we obtain the Cauchy stresses that

$$\sigma_1 = 0 \tag{6.1}$$

$$\sigma_2 = \frac{2}{3}E_sX(2\cos\alpha + \sin\alpha) \tag{6.2}$$

$$\sigma_3 = \frac{2}{3}E_sX(\cos\alpha + 2\sin\alpha) \tag{6.3}$$

The effective stress and effective strain are

$$\sigma_e = \sqrt{\frac{3}{2}s_{ij}s_{ij}} = \frac{2}{\sqrt{3}}E_sX\sqrt{1 + \frac{1}{2}\sin 2\alpha} \tag{7.1}$$

$$\varepsilon_e = \sqrt{\frac{2}{3}\varepsilon_{ij}\varepsilon_{ij}} = \frac{2}{\sqrt{3}}X\sqrt{1 + \frac{1}{2}\sin 2\alpha} \tag{7.2}$$

For a metal material characterized by a power-law hardening $\sigma = K\varepsilon^N$, the secant modulus and tangent modulus are given by

$$E_s = \frac{\sigma_e}{\varepsilon_e} = K\varepsilon_e^{N-1} \tag{8.1}$$

$$E_t = \frac{d\sigma_e}{d\varepsilon_e} = NK\varepsilon_e^{N-1} \tag{8.2}$$

Incompressible neo-Hookean model is adopted to describe the elastomer substrate, with strain energy density given by $W = \frac{E}{6}(\lambda_1^2 + \lambda_2^2 + \lambda_3^2 - 3)$, where E is the initial Young's modulus and $\lambda_i = e^{\varepsilon_i}$ ($i = 1 - 3$) is the principal stretch. Following Biot (1965), the rate form of constitutive relation for a neo-Hookean material can be given as follows

$$\bar{\sigma}_{11} = \frac{4E}{9}\lambda_1^2\dot{\varepsilon}_{11} - \frac{2E}{9}\lambda_2^2\dot{\varepsilon}_{22} - \frac{2E}{9}\lambda_3^2\dot{\varepsilon}_{33} + \dot{p} \tag{9.1}$$

$$\bar{\sigma}_{22} = -\frac{2E}{9}\lambda_1^2\dot{\varepsilon}_{11} + \frac{4E}{9}\lambda_2^2\dot{\varepsilon}_{22} - \frac{2E}{9}\lambda_3^2\dot{\varepsilon}_{33} + \dot{p} \tag{9.2}$$

$$\bar{\sigma}_{33} = -\frac{2E}{9}\lambda_1^2\dot{\varepsilon}_{11} - \frac{2E}{9}\lambda_2^2\dot{\varepsilon}_{22} + \frac{4E}{9}\lambda_3^2\dot{\varepsilon}_{33} + \dot{p} \tag{9.3}$$

$$\bar{\sigma}_{23} = \frac{E}{6}\left(\lambda_2^2 + \lambda_3^2\right)\dot{\varepsilon}_{23} + \frac{E}{6}\left(\lambda_2^2 + \lambda_3^2\right)\dot{\varepsilon}_{32} \tag{9.4}$$

$$\bar{\sigma}_{31} = \frac{E}{6}\left(\lambda_1^2 + \lambda_3^2\right)\dot{\varepsilon}_{13} + \frac{E}{6}\left(\lambda_1^2 + \lambda_3^2\right)\dot{\varepsilon}_{31} \tag{9.5}$$

$$\bar{\sigma}_{12} = \frac{E}{6}\left(\lambda_1^2 + \lambda_2^2\right)\dot{\varepsilon}_{12} + \frac{E}{6}\left(\lambda_1^2 + \lambda_2^2\right)\dot{\varepsilon}_{21} \tag{9.6}$$

Eqs. (9.1)–(9.6) can be also written in the form of $\bar{\sigma}_{ij} = L_{ijkl}\dot{\varepsilon}_{kl} + \dot{p}\delta_{ij}$, the explicit form of instantaneous moduli L_{ijkl} for neo-Hookean material are summarized in Appendix A2. The Cauchy stress in the elastomer layer is given by

$$\sigma_1 = 0 \tag{10.1}$$

$$\sigma_2 = \frac{E}{3}\left(\lambda_2^2 - \lambda_1^2\right) = \frac{E}{3}\left(e^{2\varepsilon_2} - e^{2\varepsilon_1}\right) \tag{10.2}$$

$$\sigma_3 = \frac{E}{3}\left(\lambda_3^2 - \lambda_1^2\right) = \frac{E}{3}\left(e^{2\varepsilon_3} - e^{2\varepsilon_1}\right) \tag{10.3}$$

2.2. Bifurcation analysis

A substrate/metal bilayer structure or a freestanding metal film is considered. When subjected to a subcritical in-plane biaxial loading, the structure is in the pre-bifurcation state and undergoes homogeneous deformation so that the rate equilibrium equations admit trivial solution; when the biaxial loading reaches a critical level, a non-trivial solution representing non-homogeneous deformation becomes possible to the rate equilibrium equations, indicating the onset of bifurcation instability. The critical loading triggering the bifurcation instability is named the bifurcation limit. To determine the bifurcation limit, we perform bifurcation analysis following an established procedure (Bigoni et al., 1997; Hutchinson and Tvergaard, 1980). Equilibrium and incompressibility require that

$$c_{ijkl}v_{l,ki} + p_{,j} = 0 \ (j = 1, 3) \tag{11.1}$$

$$v_{i,i} = 0 \tag{11.2}$$

where $v(x_1, x_2, x_3)$ is the velocity field and c_{ijkl} the model coefficients. It is worthwhile to mention that the development of Eqs. (11) does not rely on any prescribed constitutive law so that they are valid for both a power-law material layer and a neo-Hookean elastomer layer. Detailed derivations of the governing equations Eqs. (11) and explicit expressions of coefficients c_{ijkl} for both the power-law material and the neo-Hookean elastomer are listed in Appendix A3.

Nontrivial solutions to the governing Eqs. (11) take the form

$$v_1 = A_1 e^{zkx_1}\cos(k_2x_2)\cos(k_3x_3) \tag{12.1}$$

$$v_2 = A_2 e^{zkx_1}\sin(k_2x_2)\cos(k_3x_3) \tag{12.2}$$

$$v_3 = A_3 e^{zkx_1}\cos(k_2x_2)\sin(k_3x_3) \tag{12.3}$$

$$p = A_4 e^{zkx_1}\cos(k_2x_2)\cos(k_3x_3) \tag{12.4}$$

Here k_2 and k_3 are wavenumbers that characterize the surface undulation. A_j ($j = 1, 4$), and z are parameters, which may take real or complex values. The bifurcation limit only depends on the ratio between k_2 and k_3. Thus we can write

$$k_2 = k\cos\Omega \tag{13.1}$$

$$k_3 = k\sin\Omega \tag{13.2}$$

where k is positive and $0 \leq \Omega \leq \pi/2$. To elucidate the physical meaning of k and Ω, Fig. 1 plots the normalized out-of-plane velocity, $\cos(k\cos(\Omega)x_2)\cos(k\sin(\Omega)x_3)$, at the film surface. The color contour represents the normalized velocity value, with red being 1 and blue −1. Perspective view and top view of the checkerboard-shaped velocity field are shown in Fig. 1a and Fig. 1b–d, respectively. Upon the critical loading, any array of troughs (blue pits shown in Fig. 1) of the checkerboard-shaped velocity field may coalesce and form a necking band, which is highlighted by a black line in Fig. 1a. The wavelength between neighboring parallel necking bands along x_2 and x_3 axis is $\frac{2\pi}{k_2}$ and $\frac{2\pi}{k_3}$, respectively. The necking bands make an inclination angle $\Omega = \arctan(k_3/k_2)$ with the x_3 direction. As an example, the out-of-plane velocity field with $\Omega = 45°$ and the associated necking bands are plotted in Fig. 1b. The necking bands make an inclination angle of 45° with the x_3 direction. It is worth noting that two groups of necking bands may form for $0° < \Omega < 90°$. For $\Omega = 45°$, one group of necking bands (black lines in Fig. 1b) has an angle of 45° measured counterclockwise from the x_3 axis; and another group of necking bands (dark red lines) makes an angle of 45° measured clockwise from x_3 axis. The two groups of necking bands are symmetric with respect to the x_3 axis. Experimental evidence has confirmed the coexistence of the two symmetric clusters of necking bands (Xiang et al., 2005). Fig. 1c and d show the out-of-plane velocity field for $\Omega = 90°$ and $\Omega = 0°$, respectively. The associated necking bands are perpendicular to the x_3 axis for $\Omega = 90°$ and parallel to the x_3 axis for $\Omega = 0°$. For $\Omega = 0°$ or 90°. Only one group of necking bands exists because the necking bands and the symmetry axis coincide. In summary, k describes the wavelength of the necking pattern formed due to bifurcation and Ω prescribes the necking band orientation.

We next determine the bifurcation limit. Substituting the solution in Eq. (12) into the governing Eqs. (11) yields 4 algebraic equations for A_1, A_2, A_3 and A_4,

$$\begin{bmatrix} M_{11} & M_{12} & M_{13} & M_{14} \\ M_{21} & M_{22} & M_{23} & M_{24} \\ M_{31} & M_{32} & M_{33} & M_{34} \\ M_{41} & M_{42} & M_{43} & M_{44} \end{bmatrix} \begin{bmatrix} A_1 \\ A_2 \\ A_3 \\ A_4 \end{bmatrix} = 0 \tag{14}$$

All components M_{ij} of the matrix $\boldsymbol{M}$ depend on z, X, Ω and k. Explicit expressions of M_{ij} are listed in Appendix A4. To have nontrivial solutions, the determinant above must vanish, i.e.,

$$\det(\boldsymbol{M}) = 0 \tag{15}$$
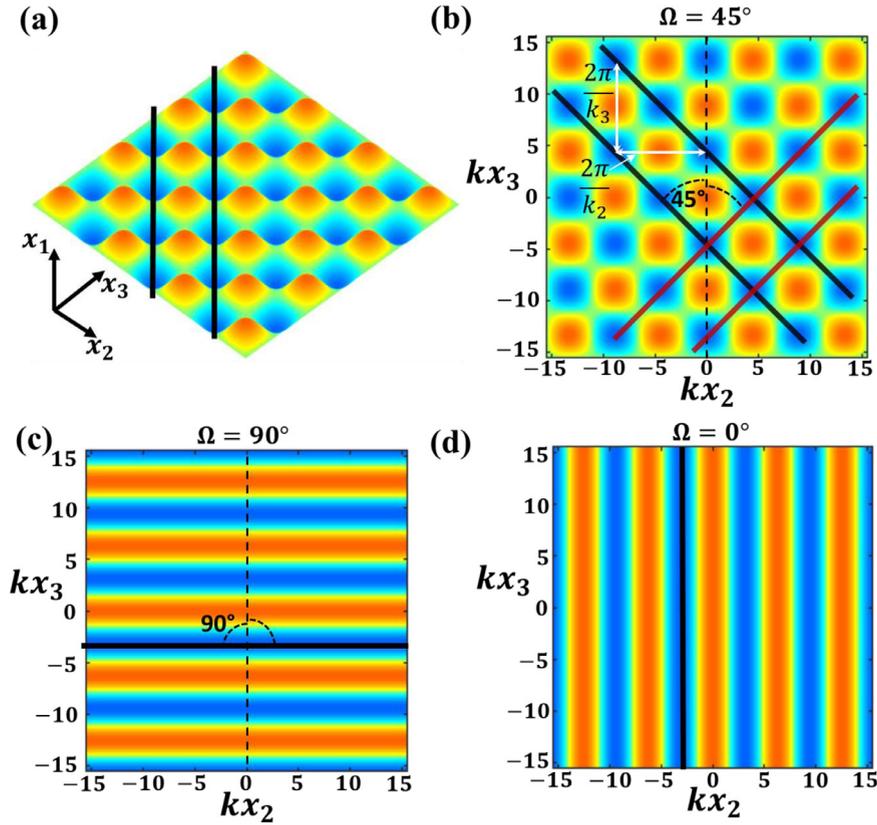
Fig. 1. Normalized out-of-plane velocity field $cos(kcos(\Omega)x_2)cos(ksin(\Omega)x_3)$ at the metal film surface. (a) Perspective view of the out-of-plane velocity field. The color contour from blue to red represents normalized velocity value ranging from -1 to 1. Top views of the normalized out-of-plane velocity field with (b) $\Omega = 45°$, (c) $\Omega = 90°$ and (d) $\Omega = 0°$ are presented. A necking band may form via the coalescence of an array of troughs of the out-of-plane velocity field. Ω specifies the necking band orientation and k describes the necking pattern wavelength. (For interpretation of the references to color in this figure legend, the reader is referred to the web version of this article.)

The vanishing determinant $det(\mathbf{M})$ leads to a cubic equation of z^2, with six complex-valued roots z that can be solved numerically. The wavenumber k can be eliminated in Eq. (15) and thus values of the six roots of z depend only on c_{ijkl} (i.e., X) and Ω. Moreover, the cubic equation of z^2 are in the elliptic range and thus there are three roots with positive real part and the other three roots with negative real part (Hutchinson and Tvergaard, 1980).

Let $A_{j(i)}$ $(j = 1, 4)$ be a normalized nontrivial solution of the Eq. (14) associated with z_i $(i = 1, 6)$. In general, they are complex-valued. Then the velocity field given in Eqs. (12) can be written as a linear combination of the six solutions $A_{j(i)}$ $(i = 1, 6)$, with $Re[]$ denoting the real part of a complex number

$$v_1 = \sum_{i=1}^{6} \xi_i Re\left[A_{1(i)}e^{z_i kx_1}\right]cos(k_2x_2)cos(k_3x_3) \tag{16.1}$$

$$v_2 = \sum_{i=1}^{6} \xi_i Re\left[A_{2(i)}e^{z_i kx_1}\right]sin(k_2x_2)cos(k_3x_3) \tag{16.2}$$

$$v_3 = \sum_{i=1}^{6} \xi_i Re\left[A_{3(i)}e^{z_i kx_1}\right]cos(k_2x_2)sin(k_3x_3) \tag{16.3}$$

$$p = \sum_{i=1}^{6} \xi_i Re[A_{4(i)}e^{z_i kx_1}]cos(k_2x_2)cos(k_3x_3) \tag{16.4}$$

ξ_i in Eqs. (16) are six constants to be determined by boundary conditions. Therefore, the bifurcation limit X and corresponding k and Ω can be obtained by solving a boundary value problem. To comprehensively understand the bifurcation instability of substrate-supported metal film structures, we need to conduct bifurcation analysis on three representative material structures, namely, a free-standing metal film, a semi-infinite metal layer (i.e., an infinitely-thick free-standing metal layer), and a metal film supported by a substrate.

Case 1. For a free-standing metal film of thickness H, there are six boundary conditions: three tractions vanish at the top surface of the film and three tractions vanish at the bottom surface of the film, i.e., $\dot{t}_{1j} = 0$ $(j = 1, 3)$ at both the top surface and bottom surface. Plugging expression of $\dot{t}_{ij}$ into six boundary conditions leads to a set of six algebraic equations for $\xi_i (i = 1, 6)$ of the form

$$\sum_{i=1}^{6} C_{ji} \xi_i = 0 \tag{17}$$

where $j = 1, 6$ and the values of C_{ji} are real. The expressions of C_{ji} are lengthy and are given in Appendix A5. They depend on X, Ω and k. To have nontrivial solutions ξ_i to Eq. (17), the determinant of the matrix $\boldsymbol{C}$ must vanish,

$$\det(\boldsymbol{C}) = 0 \tag{18}$$

This equation determines the critical X for a given wavenumber k and necking band orientation Ω. Next, we describe the detailed procedure of solving the bifurcation limit for a straining history with a fixed α: For a given combination of k and Ω within the range of $0 \leq k < \infty$ and $0 \leq \Omega \leq \pi/2$, a critical X is obtained by solving Eqs. (15) and (18) together, the critical X prescribes the critical strain at which the bifurcation mode identified by k and Ω is triggered. By screening all the k-Ω combinations in the range above, a set of critical X can be obtained as a function of k and Ω. The lowest X among all critical X's gives the bifurcation limit. The Ω and k associated with the bifurcation limit (the lowest X) specify the necking band orientation and spacing between neighboring necking bands.

Case 2. For a semi-infinite metal layer, i.e., a metal layer sitting in a semi-infinite space of $x \leq 0$, solutions shown in Eq. (16) need to remain finite when $x_1 \rightarrow -\infty$. Therefore, v_i and p are a linear combination of three solutions $A_{j(i)}$ $(j = 1, 4)$ for which z_i $(i = 1, 3)$ has a positive real part. The three boundary conditions for a semi-infinite metal layer are that three tractions equal to zero at the traction-free top surface, which gives a set of three algebraic equations for $\xi_i (i = 1, 3)$ with coefficient $\boldsymbol{C}$ defined in Appendix A6. The determinant of the coefficient matrix must vanish, $\det(\boldsymbol{C}) = 0$, to give nontrivial solutions. Then for a given history of proportional straining, the bifurcation limit of a semi-infinite metal layer can be determined by solving Eqs. (15) and (18) with matrix $\boldsymbol{C}$ given in Appendix A6.

Case 3. As the key topic of this paper, we investigate the bifurcation of the substrate/metal bilayer structure, i.e., a metal film supported by a substrate, under biaxial tension. Note that Eqs. (11)–(18) are applicable for both the metal film and the substrate, but with different values of z_i, $A_{j(i)}$ $(j = 1, 4)$, and ξ_i, denoted as z_i^+, $A_{j(i)}^+$, and κ_i^+ for the film, and z_i^-, $A_{j(i)}^-$, and ξ_i^- for the substrate. There are twelve boundary conditions for the bilayer structure: three tractions vanish at the top surface of the film, three tractions vanish at the bottom surface of the substrate, three tractions and three displacements are continuous at the interface. These boundary conditions give a set of 12 homogeneous algebraic equations for ξ_1^+, ξ_2^+, ξ_3^+, ξ_4^+, ξ_5^+, ξ_6^+, ξ_1^-, ξ_2^-, ξ_3^-, ξ_4^-, ξ_5^-, ξ_6^-, with coefficient matrix $\boldsymbol{H}$ given in Appendix A7. To have nontrivial solutions, the determinant must equal to zero, $\det(\boldsymbol{H}) = 0$. This equation together with Eq. (15) determines the critical X that triggers the bifurcation for a given combination of k and Ω. Bifurcation limit of a bilayer structure is set by the lowest X, the corresponding necking band spacing and orientation are specified by the value of k and Ω which give the lowest X.

3. Results

3.1. Bifurcation analysis of a semi-infinite metal layer

We consider a semi-infinite metal layer lying on the half-space $x_1 \leq 0$ with its top surface identified by $x_1 = 0$ and thickness being infinite. Such a semi-infinite metal layer has no characteristic length, as a result, the bifurcation limit is insensitive to the wavenumber k. Upon bifurcation, the non-uniform velocity field specified in Eq. (12) starts to develop: the top surface of the semi-infinite metal layer becomes wavy and the region near the surface experiences non-uniform deformation. Note that the non-uniform deformation prescribed by Eq. (12) decays exponentially in the thickness direction. Given the infinite thickness of the semi-infinite metal layer, the majority of the semi-infinite layer is away from the top surface and their deformation remains to be uniform. Such a bifurcation mode is defined as the *surface mode*, which eventually evolves into a series of surface cracks upon further straining beyond the bifurcation limit (Hutchinson and Tvergaard, 1980). Bifurcation of a semi-infinite metal layer is always associated with the surface mode.

Fig. 2 plots bifurcation limit in the space of ε_2 and ε_3 with various hardening indices N. Such a figure is usually referred to as bifurcation limit plot. In the plot, proportional loading with a given α corresponds to progressing along a radial line (depicted in Fig. 2 as the dotted arrow line) which makes an angle α with the axis of ε_2. The range of α in all bifurcation limit plots of this paper is from $45°$ (equibiaxial tension) to $116.6°$ (uniaxial tension). X denotes the distance from the origin. The critical bifurcation strains (i.e., $\varepsilon_2 = X \cos \alpha$ and $\varepsilon_3 = X \sin \alpha$) can be obtained from the bifurcation limit curve: For a given α and a metal of hardening index N, bifurcation occurs at the critical strains where the bifurcation limit curve of N is intersected by the dotted arrow line. The bifurcation limit curves are symmetric about the $45°$ line because switching ε_2 and ε_3 does not change the bifurcation limit. It can be concluded from Fig. 2 that an infinitely-thick metal layer with a larger hardening index has a higher bifurcation limit.
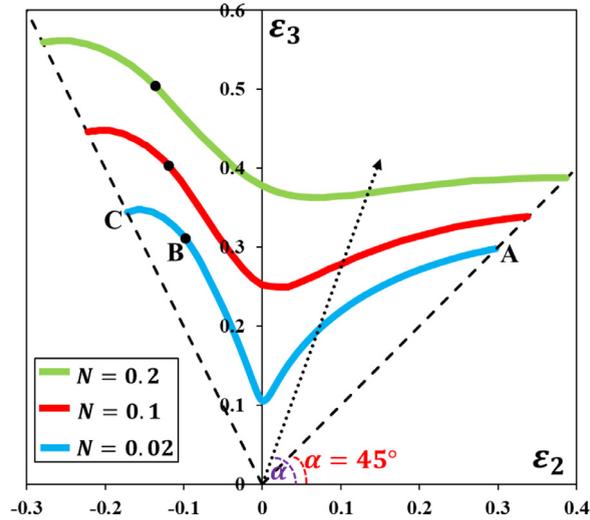
Fig. 2. Bifurcation limit plot of a semi-infinite metal layer, with its bifurcation mode being surface mode.

After analyzing the bifurcation mode and bifurcation limit, we next examine the orientation of necking bands nucleated due to the surface-mode bifurcation of semi-infinite metal layers. As aforementioned, necking bands orientation is dictated by the Ω associated with the bifurcation limit curve. For $N = 0.02$, the bifurcation limit curve (blue) is divided into two segments AB and BC by a point B identified by $\alpha \approx 107.5°$. Along the segment AB, Ω takes value of $90°$ and varies monotonically on the segment BC from $\Omega \cong 66°$ at B to $\Omega \cong 48°$ at C. It means, along AB, the necking bands are perpendicular to the ε_3 direction (i.e., the direction of larger strain, since $\varepsilon_3 > \varepsilon_2$ for $45° \leq \alpha \leq 116.6°$), while along BC necking bands are inclined to the ε_3 direction. The cases with $N = 0.1$ and $N = 0.2$ show the similar trend. The necking bands start to incline when $\alpha > 106.5°$ and $\alpha > 106°$ for $N = 0.1$ and $N = 0.2$: Ω varies monotonically from $66°$ to $46°$ for $106.5° \leq \alpha \leq 116.6°$ with $N = 0.1$, and from $70°$ to $44°$ for $106° \leq \alpha \leq 116.6°$ with $N = 0.2$. The transition point is labeled by the thick dark dot for each curve in Fig. 2. As mentioned above, bifurcation of a semi-infinite metal layer is insensitive to the wavenumber k. Therefore, the spacing between neighboring necking bands formed in a semi-infinite metal layer is arbitrary.
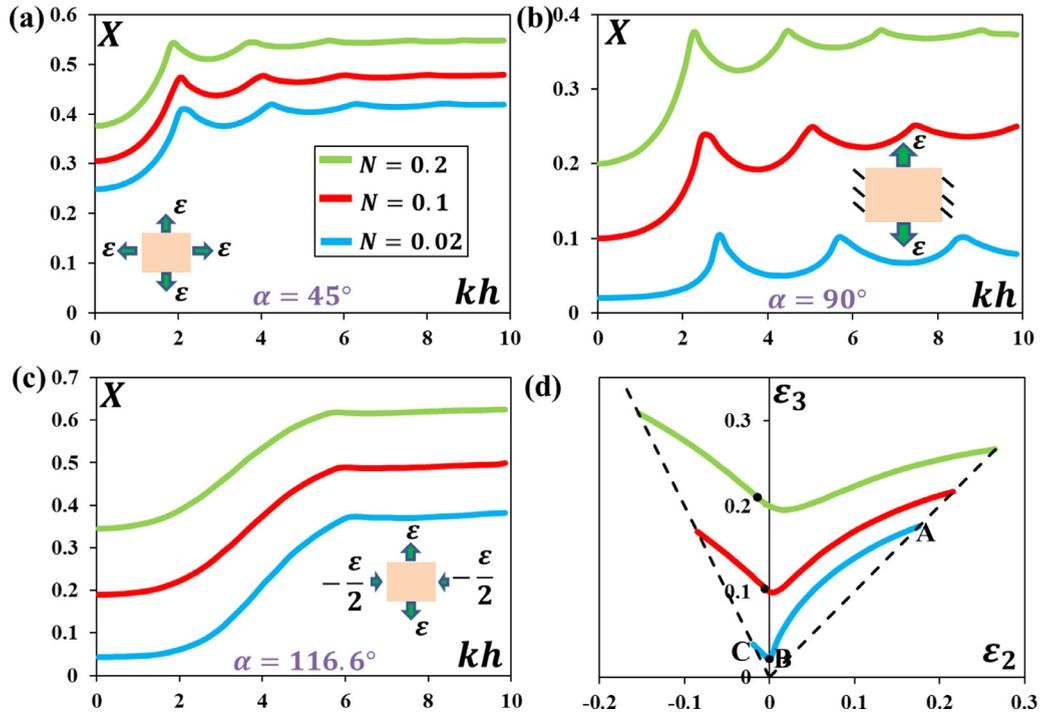
3.2. Bifurcation analysis of a free-standing metal film

We next present results of bifurcation analysis on a free-standing metal film of thickness h. To determine bifurcation limit of a free-standing metal film subjected to biaxial in-plane tension, we plot critical X as a function of dimensionless wavenumber kh, for three representative loading conditions: equi-biaxial tension with $\alpha = 45°$ (Fig. 3a), plain-strain tension with $\alpha = 90°$ (Fig. 3b) and uniaxial tension with $\alpha = 116.6°$ (Fig. 3c). It is worth noting that, in Fig. 3a–c, the critical X at a given kh corresponds to the value of Ω which minimizes X among all possible values of Ω ($0° \leq \Omega \leq 90°$).

We first check the critical X at the long wavelength limit of $kh \to 0$ and short wavelength limit of $kh \to \infty$. In the short wavelength limit, for all the three cases, the vanishing wavelength of the non-uniform deformation given by Eq. (12) developed at the film surface is trivial compared with the film thickness h and the amplitude of the non-uniform deformation decays exponentially in the thickness direction, indicating the non-uniform deformation only affects the surface layer. Therefore, the bifurcation of free-standing metal film at the short wavelength limit is corresponding to the surface mode, with critical strains (i.e., ε_2 and ε_3) approaching the surface-mode bifurcation limit given in Fig. 2. In the long wavelength limit, for plain-strain tension shown in Fig. 3b, the bifurcation analysis gives a critical strain equal to the hardening index, $\varepsilon_3 = N$, which agrees with the Considère condition.

We next check the critical X in all range of dimensionless wave number kh in order to determine the bifurcation limit. For all the three cases, the lowest critical X, the bifurcation limit, corresponds to the long wave limit of $kh \to 0$. The corresponding bifurcation mode is defined as the *single-necking mode*; as the name implies, the non-uniform deformation due to bifurcation has infinite wavelength and develops into a single necking band in the free-standing metal film when applied strain reaches the bifurcation limit. It is obvious that the bifurcation limit increases with increasing hardening index N. The critical X in all range of kh for equi-biaxial tension (Fig. 3a) and plane-strain tension (Fig. 3b) is associated with $\Omega = 90°$. But necking bands formed under uniaxial tension (Fig. 3c) corresponds to some Ω in the open range of $39° < \Omega < 55°$. In particular, the Ω related to bifurcation limit (at the long wave limit) is approximately $54.9°$, $52.5°$ and $51.9°$ for $N = 0.02$, $N = 0.1$ and $N = 0.2$, respectively.

As shown in Fig. 3d, bifurcation limit of a free-standing metal film for $45° \leq \alpha \leq 116.6°$ is plotted in the space of ε_2 and ε_3. The bifurcation limit plot summarizes information about the three key ingredients of bifurcation of a freestanding metal film under tension: the bifurcation limit determined by X, the bifurcation mode prescribed by k, and the necking

Fig. 3. Critical X at which bifurcation occurs is plotted as a function of dimensionless wavenumber kh, for three representative proportional straining conditions (a) $\alpha = 45°$, (b) $\alpha = 90°$ and (c) $\alpha = 116.6°$. (d) Bifurcation limit plot of a free-standing metal film. The bifurcation mode of a free-standing metal film is the single-necking mode.

band orientation specified by Ω. A freestanding metal film with a higher hardening index shows enhanced bifurcation limit. The bifurcation mode of freestanding metal film is single-necking mode with $kh = 0$, indicating that a free-standing metal film fails by the formation of a single necking band in response to in-plane biaxial tension. Regarding the necking band orientation Ω, for $N = 0.02$, along the segment AB, Ω is 90° and varies monotonically on the segment BC from $\Omega = 82.9°$ at B with $\alpha = 90°$ to $\Omega \cong 54.9°$ at C. For $N = 0.1$ and $N = 0.2$, the necking band starts to incline when $\alpha > 92.6°$ and $\alpha > 94°$, as highlighted by the black dot.

3.3. Bifurcation analysis of a metal film on an elastomer substrate

We consider an elastomer/metal bilayer structure, which is characterized by three dimensionless parameters: hardening index N, thickness ratio H_s/H_f and stiffness ratio E/K between the substrate and the film. In making Fig. 4, the stiffness ratio is taken to be $E/K = 1.05$ and the hardening index is $N = 0.02$. We vary the thickness ratio: $H_s/H_f = 1$ or 5 to elucidate the effect of substrate thickness on the bifurcation instability of the elastomer/metal bilayer.

Fig. 4 plots the critical X of the bilayer as a function of the dimensionless wavenumber kH_f for the three representative straining conditions. A curve for the freestanding metal film (blue lines) is included in Fig. 4 for comparison purposes. At a given kH_f, critical X is obtained by finding the Ω which minimizes X. In the short wave limit $kH_f \rightarrow \infty$, for $H_s/H_f = 1$ (red lines) and 5 (green lines), the non-uniform deformation with trivial wavelength only affects the surface layer of the metal film and thus does not sense the existence of the underlying elastomer substrate; the critical X approaches the short-wave limit of the free-standing metal film (i.e., the surface-mode limit of a semi-infinite metal layer), as highlighted by the dash-dotted line in Fig. 4. In the long wave limit $kH_f \rightarrow 0$, in stark contrast with the freestanding metal film, the critical X of the bilayer for single-necking bifurcation mode becomes infinite as shown by the dotted line (green and red) in Fig. 4b. Instead, the bifurcation mode for the bilayer at the long wave limit $kH_f \rightarrow 0$ is associated with the shear-band formation, with the corresponding critical X termed as the elliptic limit (Bigoni et al., 1997; Hutchinson and Neale, 1978). The elliptic limit is also insensitive to the wavenumber and is represented by the black dashed line in Fig. 4a–c.

For $H_s/H_f = 1$ (red lines), with all the three representative straining conditions including equi-biaxial tension (Fig. 4a), plane-strain tension (Fig. 4b) and uniaxial tension (Fig. 4c), the critical X remains at the elliptic limit for small kH_f, and drops precipitously as the wavenumber increases, reaching the lowest X for bifurcation at an intermediate value of kH_f. Bifurcation occurs at $kH_f = 0.9$, 1.15 and 1.9 for $\alpha = 45°$ (equi-biaxial), 90° (plane-strain) and 116.6° (uniaxial), respectively. The bifurcation mode with a non-zero finite kH_f corresponds to the formation of multiple periodic necking bands, therefore the bifurcation mode of the substrate-supported metal film is classified as the *multiple-necking mode*. Further increasing the substrate thickness complicates the bifurcation mode. For a bilayer with $H_s/H_f = 5$ (green lines) under plane-strain (Fig. 4b)
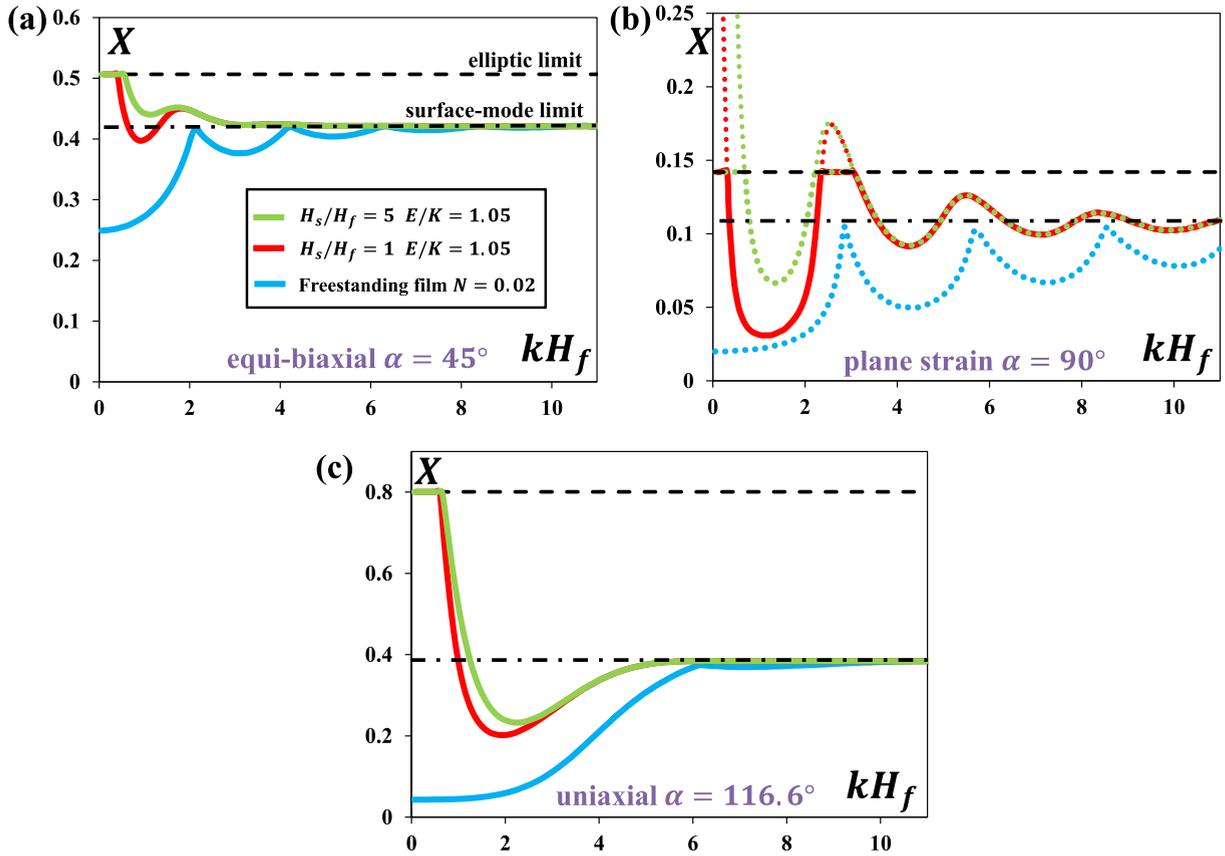
Fig. 4. Critical X of an elastomer/metal bilayer is plotted as a function of kH_f for various proportional straining conditions (a) $\alpha = 45°$, (b) $\alpha = 90°$ and (c) $\alpha = 116.6°$. To show the effect of substrate thickness on the bifurcation of the bilayer, thickness ratio is varied from 0 (free-standing metal film) to 1 and 5.

or uniaxial tension (Fig. 4c), minimum X is reached at a non-zero finite kH_f and thus the bifurcation is associated with multiple-necking mode; while under equi-biaxial tension (Fig. 4a), X minimizes at $kH_f \to \infty$ which is corresponding to the surface mode. Fig. 4a–c also compares the bifurcation limit X of elastomer/metal bilayer to that of the freestanding metal film. It is evident that the presence of the elastomer substrate enhances the bifurcation limit: the thicker the substrate, the higher the bifurcation limit X.

Critical Ω associated with curves in Fig. 4 is determined by finding the Ω which minimizes X at a given kH_f. Similar to that of a free-standing metal film, for equi-biaxial tension (Fig. 4a) and plane-strain tension (Fig. 4b), the bifurcation of elastomer/metal bilayers corresponds to $\Omega = 90°$ for any kH_f. The associated necking bands are always transverse to the x_3 axis (the direction with larger strain); For uniaxial tension (Fig. 4c), Ω is in the range of $47° \leq \Omega \leq 56°$ for $H_s/H_f = 1$ and $47° \leq \Omega \leq 57°$ for $H_s/H_f = 5$, indicating the formation of slanted necking bands. The Ω related to the bifurcation limit (lowest X) is approximately $54°$, $52°$ and $51°$ for $H_s/H_f = 0$ (free-standing metal film), $H_s/H_f = 1$ and $H_s/H_f = 5$, respectively. It can be concluded that the elastomer substrate not only affects the bifurcation mode and corresponding bifurcation limit, but it also changes the orientation of the developed necking bands.

Fig. 5 shows the bifurcation limit plots of an elastomer-supported metal layer, for three different values of $N = 0.02$ (Fig. 5a), 0.1 (Fig. 5b), and 0.5 (Fig. 5c), respectively. Stiffness ratio E/K is fixed to 1.05. We will elaborate on the effect of substrate thickness on the bifurcation limit of metal films in four aspects:

(1) Bifurcation retardation: Fig. 5a shows three bifurcation limit curves corresponding to $H_s/H_f = 0$ (free metal film), 1, and 5. Here, $N = 0.02$. For each curve, it is evident that the bifurcation limit strain ε_3 under plane-strain tension ($\varepsilon_2 = 0$) is lower than those under equibiaxial tension and uniaxial tension. For example, when $H_s/H_f = 1$, the critical necking limit strains ε_3 are 0.28, 0.03, and 0.18, for $\alpha = 45°$ (equi-biaxial), $90°$ (plane-strain) and $116.6°$ (uniaxial), respectively. In this sense, previous studies assuming plane-strain condition tend to underestimate the bifurcation limit of the metal layers on elastomer substrate subject to uniaxial tensile loading (Li and Suo, 2006). Fig. 5a compares curves with various thickness ratios: for any given α, the bifurcation strain of an elastomer-supported metal film is higher than that of the freestanding metal film. In other words, the necking is retarded to occur at a higher strain by the elastomer substrate.
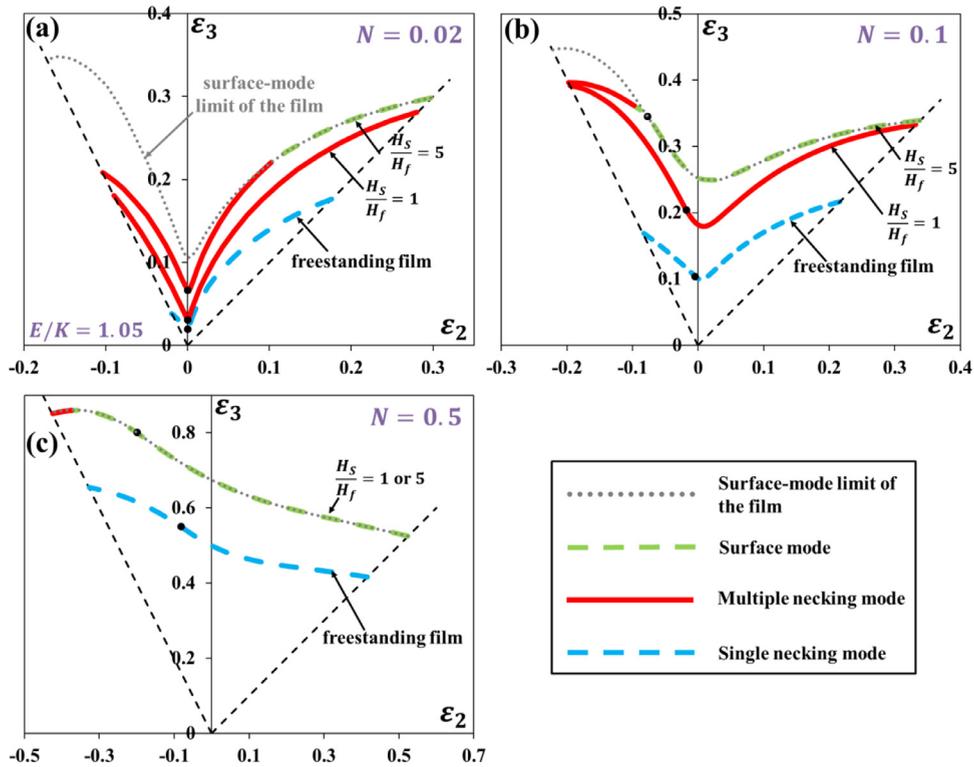
Fig. 5. Bifurcation limit plots of elastomer-supported metal layers with various H_s/H_f. The stiffness ratio $E/K = 1.05$. (a) Hardening index N of metal layer is 0.02 (a), 0.1 (b) and 0.5 (c), respectively. Three distinct bifurcation modes, including single-necking mode, multiple-necking mode and surface mode, are represented by blue dashed line, red solid line, and green dashed line, respectively. Theoretical upper bound of bifurcation limit of substrate/metal bilayers is delineated (grey dotted lines). (For interpretation of the references to color in this figure legend, the reader is referred to the web version of this article.)

The thicker the substrate, the more significant retardation of bifurcation occurrence. Similar bifurcation retardation effect and its dependence on H_s/H_f are evident in Fig. 5b and c, in which $N = 0.1$ and $N = 0.5$, respectively.

(2) Bifurcation mode: As shown in Fig. 4, at the three representative straining conditions, there exist three possible critical bifurcation modes for the elastomer/metal bilayer structure: single-necking mode, multiple-necking mode, and surface mode. For example, single-necking mode occurs in free-standing metal films; multiple-necking mode dominates in elastomer/metal bilayer with $H_s/H_f = 1$ and 5 under plane-strain and uniaxial straining; Surface mode prevails for bilayer with a thick substrate ($H_s/H_f = 5$) under equi-biaxial tension. Bifurcation modes of bilayers in all range of α are presented in Fig. 5. Fig. 5a–c shows critical bifurcation modes of elastomer/metal bilayers. With the stiffness ratio and hardening index fixed, the bifurcation modes are affected by the thickness ratio and the straining ratio angle α. In general, for a given α, when substrate thickness increases, bifurcation mode of elastomer/metal bilayer tends to transit from single-necking mode, to multiple-necking mode, and finally to the surface mode. The condition under which a bifurcation mode occurs is summarized as follows: (i) Single-necking mode (blue dashed line in Fig. 5): As shown in Fig. 5, single-necking mode prevails in free-standing metal film with any hardening index at any α ($45° \leq \alpha \leq 116.6°$). (ii) Multiple-necking mode (red solid line in Fig. 5): Elastomer/metal bilayer with thin substrate tend to undergo multiple-necking mode. For example, for bilayers with weakly hardening metal ($N = 0.02$ in Fig. 5a and $N = 0.1$ in Fig. 5b), multiple-necking mode is prevailing for thickness ratio of $H_s/H_f = 1$ at any straining angle $45° \leq \alpha \leq 116.6°$; Elastomer/metal bilayers with thick substrate only experience multiple-necking mode at large α. For $H_s/H_f = 5$, multiple-necking mode occurs at $51.1° \leq \alpha \leq 116.6°$ for $N = 0.02$ (Fig. 5a), $105.1° \leq \alpha \leq 116.6°$ for $N = 0.1$ (Fig. 5b), and $113.5° \leq \alpha \leq 116.6°$ for $N = 0.5$ (Fig. 5c), respectively. (iii) Surface mode (green dashed line in Fig. 5): surface mode appears only when the substrate becomes thick. For instance, surface mode occurs in laminates with $H_s/H_f = 5$ and $N = 0.02$ when $45° \leq \alpha < 65.1°$ (Fig. 5a); and in laminates with $H_s/H_f = 5$ and $N = 0.1$ when $45° \leq \alpha < 105.1°$ (Fig. 5b).

(3) Upper bound of bifurcation limit of elastomer/metal bilayer: Bifurcation retardation effect of the elastomer substrate is attributed to the mechanical constraint of the substrate to the metal film. Strong mechanical constraint from the thick substrate leads to high resistance for the occurrence of necking bands, giving rise to suppression of single/multiple-necking mode and thus enhanced bifurcation limit corresponding to surface mode (e.g. curves of $H_s/H_f = 5$ in Fig. 5). It is important to realize that the surface mode bifurcation only affects deformation in an infinitesimally thin region underneath the metal film surface. Considering the finite thickness of the film, the infinitesimally thin region does not sense the existence of the substrate. It implies that the elastomer substrate cannot influence the bifurcation limit when the
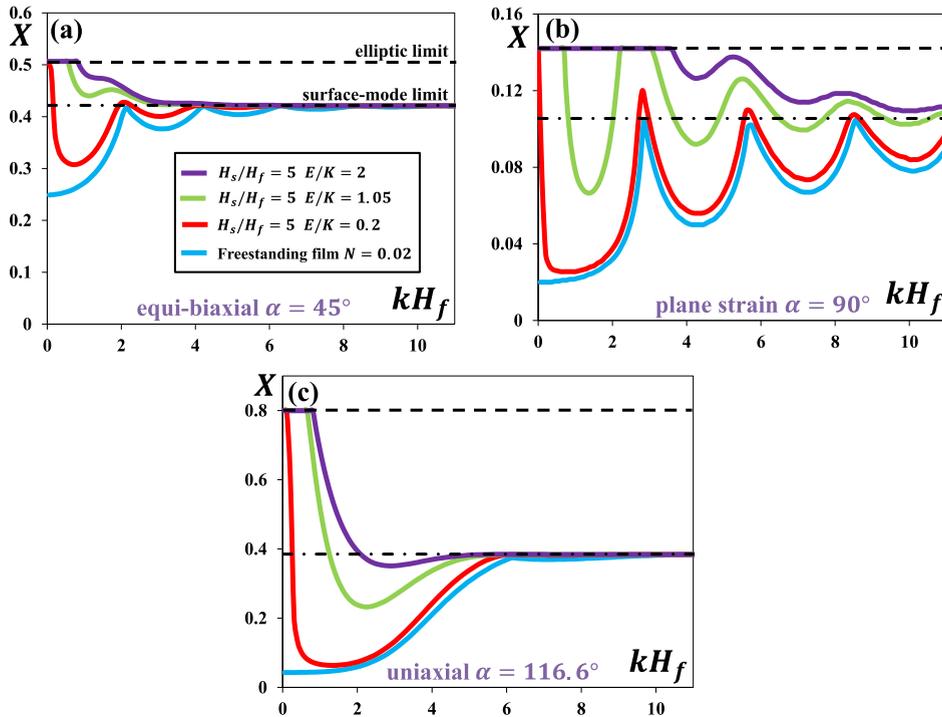
Fig. 6. Critical X is plotted as a function of kH_f to show the effect of substrate stiffness on the bifurcation of the elastomer/metal bilayer, for three representative straining conditions (a) $\alpha = 45°$, (b) $\alpha = 90°$ and (c) $\alpha = 116.6°$.

surface mode becomes the dominating bifurcation mode of the elastomer/substrate bilayer. In other words, the surface-mode bifurcation limit of the metal film sets the theoretical upper bound for bifurcation limit of the elastomer/metal bilayer: No matter how thick the substrate is, the bifurcation limit of the elastomer/metal bilayer cannot be increased beyond the surface-mode limit of the metal film itself. In Fig. 5, it is evident that bifurcation limit curves of elastomer/metal bilayers are capped by the theoretical upper bounds (grey dotted line), the surface-mode bifurcation limit of the metal film. In Fig. 5c, for $N = 0.5$, bifurcation limit curves with $H_s/H_f = 1$ and $H_s/H_f = 5$ coincide with the upper bound curve for $45° \leq \alpha \leq 113.5°$; it indicates that once the upper bound is reached (with $H_s/H_f = 1$), further increasing the substrate thickness (to $H_s/H_f = 5$) does not enhance the bifurcation limits, which is in line with the analysis above.

(4) Necking band orientation: To show the necking band orientation Ω, in Fig. 5, each bifurcation limit curve is divided into two segments by a black dot. The right segment is corresponding to $\Omega = 90°$ with necking bands occurring along a direction $90°$ away from (i.e. perpendicular to) the x_3 direction; while the left segment corresponds to some Ω in the open range of $0 < \Omega < \pi/2$ and the necking bands appear along a slanted direction. For example, in Fig. 5b, for the bilayer with $H_s/H_f = 1$, Ω varies from $83.9°$ to $47.9°$ for $97.6° \leq \alpha \leq 116.5°$, where $\alpha = 97.6°$ corresponds to the black dots. Necking band orientation angle has been extensively studied in uniaxial-tensile experiments of substrate-supported metal layers (Gruber et al., 2004; Lu et al., 2010). For example, necking bands in a thin copper film (170 nm thick) supported by a polyimide substrate (100 μm) exhibit an inclination angle about $60°$ away from the uniaxial tension direction (Xiang et al., 2005). Our calculation shows that for $N = 0.02$, under uniaxial tension ($\alpha = 116.6°$), $\Omega = 54.9°$, $52.9°$, and $50.9°$ for $H_s/H_f = 0$, 1 and 5, respectively, which agrees reasonably well with the experiments.

Effect of substrate stiffness on the bifurcation limit is shown in Figs. 6 and 7 with thickness ratio fixed at $H_s/H_f = 5$. Fig. 6 shows X as a function of kH_f with $E/K = 0$ (Free-standing metal layer), 0.2, 1.05, and 2 for the three representative straining conditions. The effect of bifurcation retardation becomes more significant as the substrate stiffness E/K increases. The stiffer the substrate, the higher the bifurcation limit. Fig. 6 further reveals the effect of substrate stiffness on the bifurcation mode. With increasing E/K, bifurcation mode of elastomer/metal bilayer tends to transit from single-necking mode, to multiple-necking mode, and finally to the surface mode. For example, under equi-biaxial tension (Fig. 6a), the bifurcation of elastomer/metal bilayers corresponds to single-necking mode for $E/K = 0$, multiple-necking mode for $E/K = 0.2$, and surface mode for $E/K = 1.05$ and 2. A similar transition in bifurcation mode is evident in Fig. 6b and c. As abovementioned, bifurcation limit of elastomer/metal bilayer is capped by the surface-mode limit of the metal film. Therefore, once the critical bifurcation limit reaches the surface-mode limit, further increasing the substrate stiffness cannot raise the bifurcation limit, as exemplified by the green and purple lines shown in Fig. 6a.

Bifurcation limit plots with various stiffness ratios and metal hardening indices are shown in Fig. 7. Fig. 7a shows four bifurcation limit curves for $N = 0.02$ corresponding to $E/K = 0$, 0.2, 1.05, and 2. Single-necking mode, multiple-necking mode,
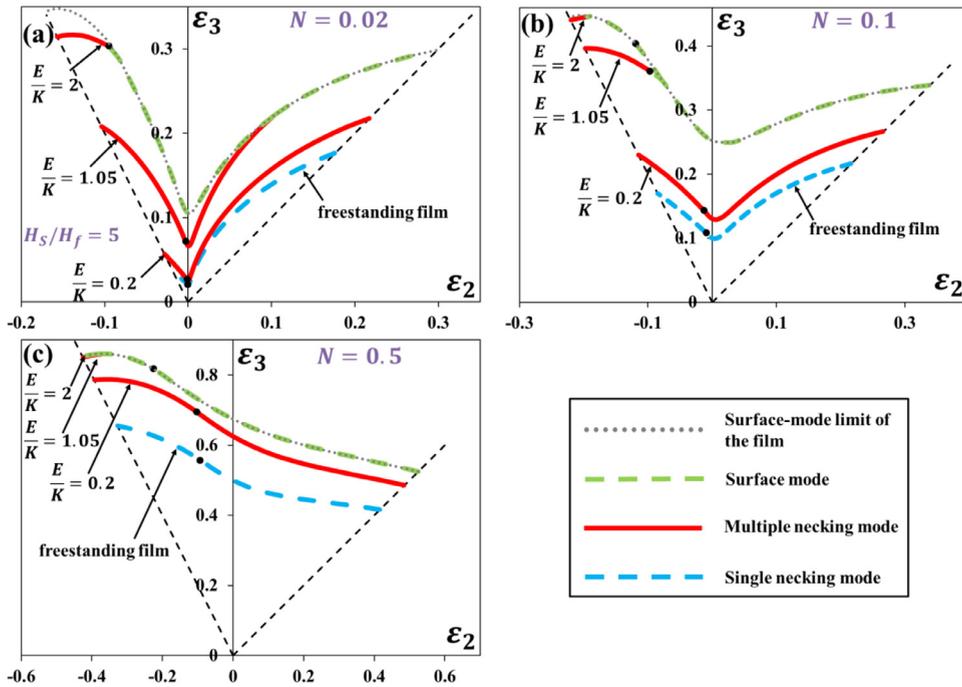
Fig. 7. Bifurcation limit plot of elastomer-supported metal layer with various E/K. Hardening index N of metal layer is (a) 0.02, (b) 0.1 and (c) 0.5. Thickness ratio is taken to be $H_s/H_f = 5$.

and surface mode are highlighted by blue, red, and green lines, respectively. Bifurcation of an elastomer/metal bilayer can be retarded to a higher strain by attaching the metal film to a stiffer elastomer substrate. Bifurcation modes are strongly affected by the substrate stiffness. Single-necking mode is the critical bifurcation mode for freestanding metal film, while multiple-necking mode dominates for bilayers with complaint substrate of $E/K = 0.02$, as demonstrated in Fig. 7a–c. Further increasing the substrate stiffness (to $E/K = 1.05$) raises the bifurcation limit curve to the theoretical upper bound for a certain range of α and thus surface mode starts to set in. For example, in Fig. 7a, when $E/K = 1.05$ surface mode occurs at small straining ratio angle $45° \leq \alpha \leq 65.1°$. The surface mode becomes more prevailing as the substrate becomes stiffer. In Fig. 7a, when $E/K = 2$, the occurrence of the surface mode is associated with straining ratio angle of $45° \leq \alpha \leq 107.5°$. As the bifurcation limit of elastomer/metal bilayer is capped by the surface-mode limit of the metal film, bifurcation limit curves of $E/K = 1.05$ and $E/K = 2$ partially coincide for $45° \leq \alpha \leq 65.1°$. Fig. 7b and c shows similar feature: bifurcation limit curves of $E/K = 1.05$ and $E/K = 2$ partially coincide for $45° \leq \alpha \leq 102.6°$ and $45° \leq \alpha \leq 112.5°$ for $N = 0.1$ and 0.5, respectively, because of the fact that they reach the theoretical upper bound set by the surface-mode limit of metal film.

The effect of substrate thickness and stiffness on the bifurcation retardation and bifurcation mode can be physically understood as follows. The elastomer substrate that follows a neo-Hookean constitutive law by itself does not suffer from bifurcation instability, including single-necking mode, multiple-necking mode, and surface mode. So the elastomer substrate provides mechanical constraints to resist bifurcation-induced localized deformation in the metal film, and thus retards the occurrence of bifurcation, carrying the metal film to deform uniformly to a large strain. For single-necking bifurcation mode, the elongation of the metal film is accommodated by large local elongation of a single necking band. Such severe strain localization is not favorable since the elastomer substrate tends to delocalize the deformation of the metal film. Compared to the single-necking mode, multiple-necking mode is associated with necked regions that are less deformed, because the overall elongation of the metal film is carried by an array of necking bands rather than a single one. As a result, in presence of a thin and compliant substrate, multiple-necking mode overwhelms the single-necking mode. Moreover, if the elastomer substrate is sufficiently stiff and/or thick, its mechanical constraint to the metal film can be sufficiently strong to completely suppress the formation of necking bands, making surface mode the bifurcation mode. As discussed above, surface mode bifurcation only affects the metal surface layer and does not sense the existence of the elastomer substrate. Therefore, surface-mode bifurcation limit cannot be further enhanced by tuning the substrate, no matter how thick and stiff the substrate is.

3.4. Bifurcation analysis of a metal film on a plastic substrate

The necking limit of a plastic/metal bilayer depends on four parameters: the hardening indices of the metal N_f and N_s, the thickness ratio H_s/H_f, and the stiffness ratio K_s/K_f. We first explore the influence of K_s/K_f on the bifurcation limit by fixing other parameters. Fig. 8a–c plots the critical X as a function of kH_f, for the combination of $N_f = 0.1$, $N_s = 0.3$, and
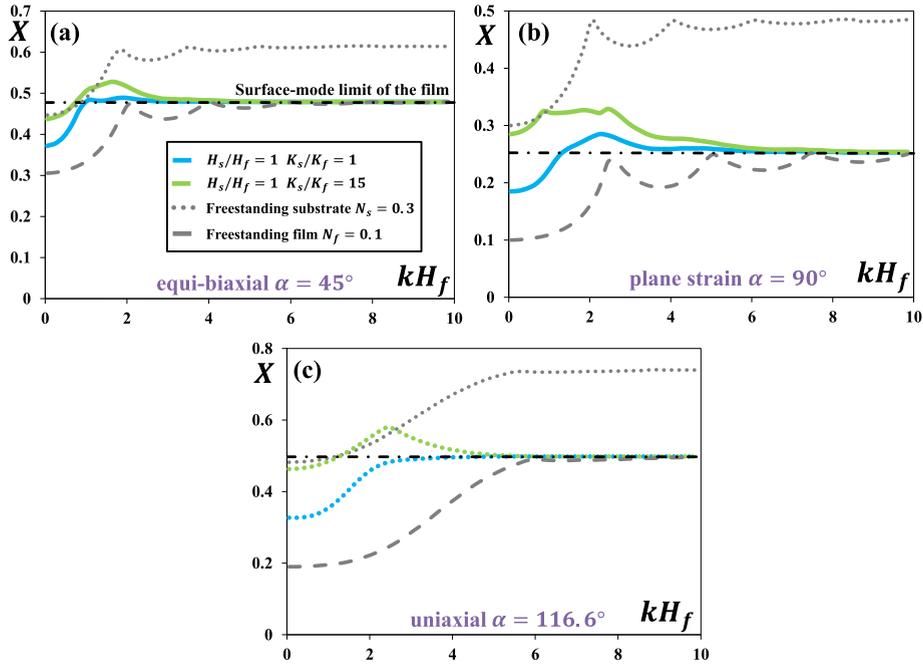
Fig. 8. Critical X is plotted as a function of kH_f to show the effect of substrate stiffness on the bifurcation limit of plastic/metal bilayers, for three representative straining conditions (a) $\alpha = 45°$, (b) $\alpha = 90°$ and (c) $\alpha = 116.6°$. Thickness ratio is taken to be $H_s/H_f = 1$. The grey dashed line and dotted line represent a freestanding film of $N_f = 0.1$ and a freestanding substrate of $N_s = 0.3$.

$H_s/H_f = 1$. Similar to that in an elastomer-supported metal layer, lowest X (i.e., bifurcation limit) of a plastic-supported metal film increases with increasing stiffness of the plastic substrate. Specifically, at equi-biaxial tension, Fig. 8a shows bifurcation limit equals to 0.372 (single-necking mode), and 0.437 (single-necking mode) for $K_s/K_f = 1$, and $K_s/K_f = 15$, respectively. At plane-strain tension (Fig. 8b), bifurcation limit is 0.185 (single-necking mode), and 0.254 (surface mode) for $K_s/K_f = 1$, and $K_s/K_f = 15$, respectively. At uniaxial tension (Fig. 8c), critical X takes value of 0.327 (single-necking mode), and 0.463 (single-necking mode) for $K_s/K_f = 1$, and $K_s/K_f = 15$, respectively. For equi-biaxial tension and plane-strain tension, the necking band always occurs in the direction perpendicular to x_3 direction that of the greater tensile strain ($\Omega = 90°$). While under uniaxial tension, the necking band appears in a slanted direction with $\Omega = 46°$ for both $K_s/K_f = 1$, and $K_s/K_f = 15$.

Fig. 9 shows bifurcation limit curves with different stiffness ratios $K_s/K_f = 0, 1, 15$. Bifurcation of plastic-supported metal films shows similarity with that of elastomer-supported metal films in two folds: (1) Bifurcation retardation effect: Comparison among the curves in Fig. 9 shows that the bifurcation is retarded to occur at a higher strain in presence of the plastic substrate. The effect of bifurcation retardation becomes more significant as K_s/K_f increases. (2) Necking band orientation: Each bifurcation curve is divided into two segments by a black dot in Fig. 9, with the right segment corresponding to necking bands perpendicular to the x_3 direction and the left segment corresponding to inclined necking bands.

Fig. 9 also reveals two distinctions between elastomer-supported metal films and plastic-supported metal films. (1) Bifurcation mode: It is important to note that one important distinction between elastomer-supported metal layers and plastic-supported metal layers lays in the bifurcation mode: plastic-supported metal layers are much more prone to the single-necking mode than elastomer-supported metal layers. For example, in Fig. 9a, plastic/metal bilayers (of $K_s/K_f = 1$ and 15) experience single-necking mode at any straining ratio angle α. It can be attributed to the fact that constraint on necking formation from plastic substrates (characterized by the power-law plasticity) is not as strong as that from elastomer substrates. (2) Theoretical upper bound of bifurcation limit of the bilayer: As discussed above, the upper bound of bifurcation limit of an elastomer-supported metal film is determined by the surface-mode bifurcation limit of the metal film. In contrast, for plastic-supported metal film, because the plastic substrate is also vulnerable to necking formation when subjected to tension, bifurcation limit of plastic-supported metal film is not only constrained by the surface-mode limit of the metal film, but it is also limited by the single-necking limit of the freestanding plastic substrate itself. Competition between surface-mode limit of the metal film and single-necking limit of a freestanding plastic substrate determines the upper bound of the bifurcation limit: the one reached by the radial proportional straining path first sets the upper bound at α. In Fig. 9a with $N_s = 0.2$ and $N_f = 0.1$. The limiting case of $K_s/K_f = \infty$ corresponds to single-necking limit curve of a freestanding plastic substrate (purple dotted line), whose bifurcation limit strains ε_3 are 0.308 (uniaxial), 0.2 (plane-strain), and 0.266 (equi-biaxial), respectively. Note that for the surface-mode limit curve of metal film with $N_f = 0.1$ (Fig. 2 and grey dotted line in Fig. 9a), the surface-mode bifurcation limit strains ε_3 are 0.446 (uniaxial), 0.252 (plane-strain), and 0.339 (equi-biaxial).
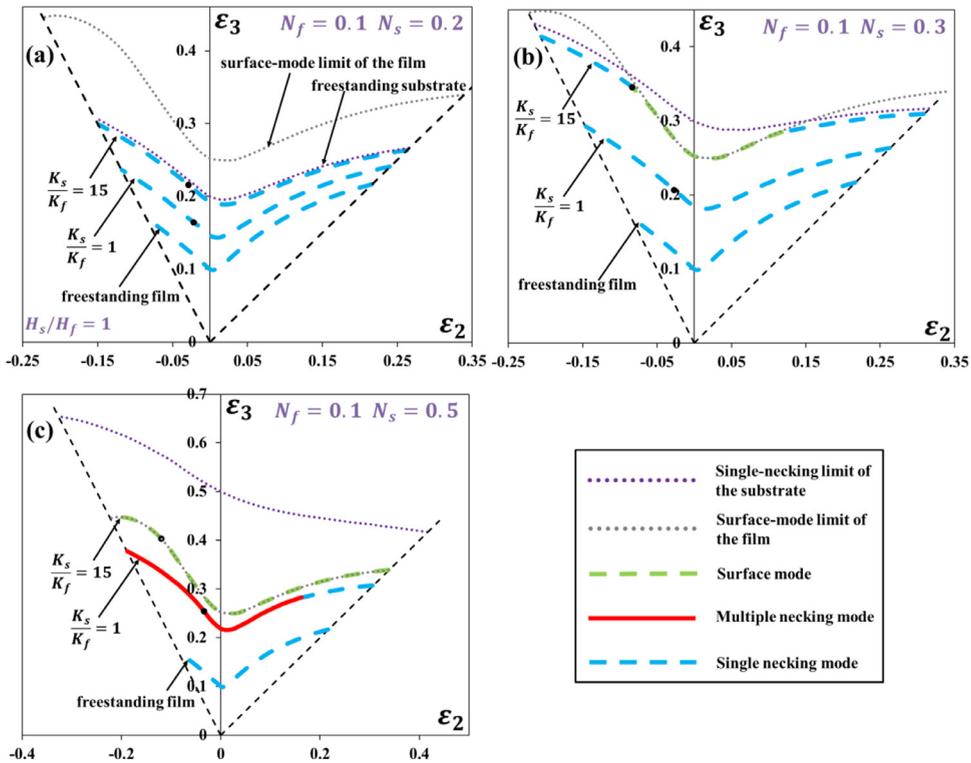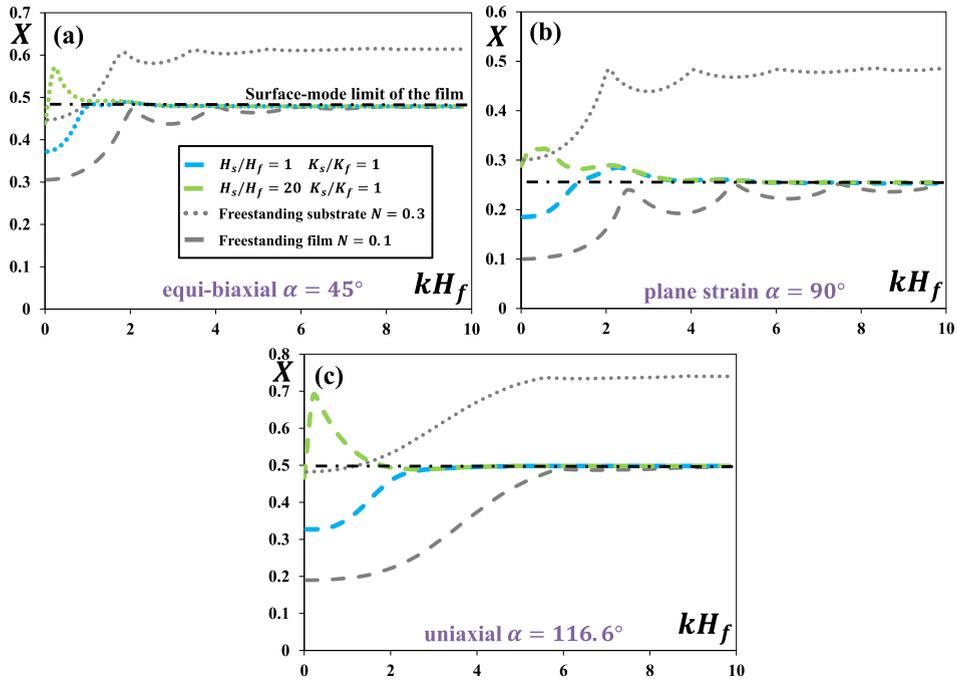
Fig. 9. Bifurcation limit plot of plastic-supported metal layers with various stiffness ratio K_s/K_f. Hardening index of the film is $N_f = 0.1$. Hardening index of the metal layer N_s is (a) 0.2, (b) 0.3 and (c) 0.5, respectively. $H_s/H_f = 1$ is used in making the plot.
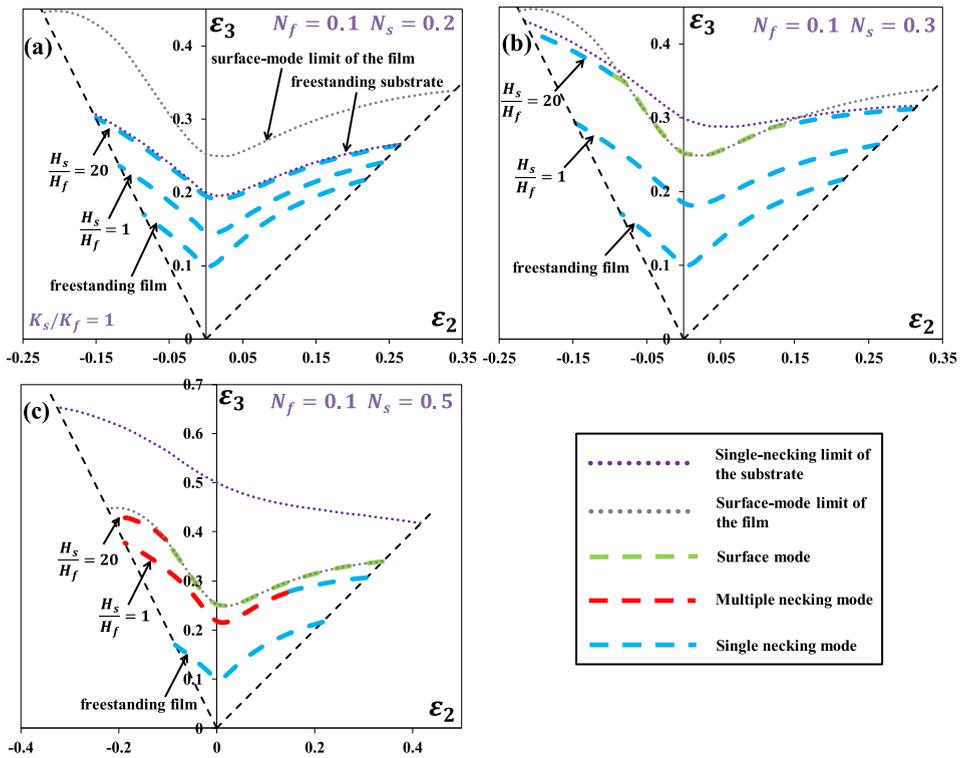
The single-necking bifurcation limit of the plastic substrate with $N_s = 0.2$ is lower than the surface-mode limit of the metal film for all range of $45° \leq \alpha \leq 116.6°$. In this case, the effect of the plastic substrate on necking retardation is capped by the single-necking bifurcation limit of the substrate itself. As exemplified in Fig. 9a, bifurcation limit curve of $K_s/K_f = 15$ is very close to but cannot be higher than the single-necking limit curve of the plastic substrate (purple dotted line in Fig. 9a). Fig. 9b shows bifurcation limit curves for the combination of $N_s = 0.3$ and $N_f = 0.1$. Note that the single-necking limit curve of the freestanding plastic substrate with $N_s = 0.3$ (purple dotted line) and the surface-mode limit curve of the metal film with $N_f = 0.1$ (grey dotted line) intersect. For a given α, the lower value of the two curves gives the theoretical upper bound of bifurcation limit of plastic-supported metal layer. The determined upper bound curve consists of three segments: one segment on the surface-mode limit curve of the metal layer at $65.1° \leq \alpha \leq 103°$ and two segments on the single-necking bifurcation limit curve of the substrate at $45° \leq \alpha < 65.1°$ and $103° < \alpha \leq 116.6°$. Fig. 9b demonstrates that stiff substrate with $K_s/K_f = 15$ is sufficiently strong to increase the bifurcation limit to the upper bound at straining angle of $67.6° \leq \alpha \leq 102.6°$. Fig. 9c plots bifurcation limit curves for $N_s = 0.5$ and $N_f = 0.1$. In this case, the surface-mode limit of the metal layer of $N_f = 0.1$ is always lower than the single-necking limit of the substrate of $N_s = 0.5$, and thus specifies the upper bound for bifurcation limit curve. The plastic substrate with $N_s = 0.5$ and $K_s/K_f = 15$ is strong enough to raise the bifurcation limit of plastic-supported metal layer to the upper bound, the surface-mode limit of the metal film, as indicated in Fig. 9.

We next study the influence of substrate thickness H_s/H_f on the bifurcation limit of plastic/metal bilayers. For the three representative straining conditions, critical X as a function of kH_f is plotted in Fig. 10a (equi-biaxial), 10b (plane-strain) and 10c (uniaxial), with $N_f = 0.1$, $N_s = 0.3$, and $K_s/K_f = 1$. Similar to the effect of substrate stiffness, increasing substrate thickness not only retards the bifurcation to occur at a higher X, but it also affects the bifurcation modes and necking band orientation. At equi-biaxial tension, Fig. 10a shows critical X equals to 0.372 (single-necking mode), and 0.44 (single-necking mode) for $H_s/H_f = 1$, and $H_s/H_f = 20$, respectively. The corresponding necking bands are perpendicular to ε_3 direction ($\Omega = 90°$). At plane-strain tension (Fig. 10b), critical X is 0.185 (single-necking mode), and 0.255 (surface mode) for $H_s/H_f = 1$, and $H_s/H_f = 20$, respectively. The corresponding necking bands also occur in the direction perpendicular to ε_3 ($\Omega = 90°$). At uniaxial tension (Fig. 10c), critical X takes value of 0.327 (single-necking mode), and 0.467 (single-necking mode) for $H_s/H_f = 1$, and $H_s/H_f = 20$, respectively. The necking band appear in a slanted direction with $\Omega = 52°$ and $\Omega = 50°$ for both $H_s/H_f = 1$, and $H_s/H_f = 20$.

Fig. 11 shows bifurcation limit curves with different thickness ratios $H_s/H_f = 1$ or 20. The effect of the substrate thickness on the bifurcation limit of the bilayer is similar to that of the substrate stiffness: the larger the substrate thickness, the higher the bifurcation limit of the plastic/metal bilayer. No matter how stiff the substrate is, the bifurcation limit of the

Fig. 10. Critical X is plotted as a function of kH_f to show the effect of substrate thickness on the bifurcation limit of plastic/metal bilayers, for three representative straining conditions (a) $\alpha = 45°$, (b) $\alpha = 90°$ and (c) $\alpha = 116.6°$. The stiffness ratio $K_s/K_f = 1$. The grey dashed line represents single-necking limit of a freestanding film of $N_f = 0.1$ and the grey dotted line is the single-necking limit curve of a freestanding substrate of $N_s = 0.3$.

Fig. 11. Bifurcation limit plot of plastic-supported metal layer with various thickness ratio H_s/H_f. Hardening index of the metal film is $N_f = 0.1$. Hardening index of the plastic substrate N_s is (a) 0.2, (b) 0.3 and (c) 0.5. Here, $K_s/K_f = 1$.

plastic/metal bilayer is capped by the upper bound determined by the competition between the surface-mode limit of the metal film and the single-necking limit of the freestanding plastic substrate. For the thickness ratio of $H_s/H_f = 20$, the bifurcation limit of the plastic/metal bilayer is very close to the theoretical upper bound. It implies that further increasing the substrate thickness cannot substantially enhance the bifurcation limit of the plastic/metal bilayer but only increases the weight of the structure, which offers a guideline for designing plastic/metal bilayer with both large bifurcation limit and low weight.

4. Conclusions and remarks

An all-wavelength bifurcation analysis is conducted to understand the onset of bifurcation instability of substrate-supported metal layers under biaxial in-plane loading over the range of straining ratio angle from $\alpha = 45°$ (equi-biaxial), to $90°$ (plane-strain), and to $116.6°$ (uniaxial). Major findings of the present study are recapped as follows:

- *Bifurcation modes*: Three different bifurcation modes are defined based on the value of wavenumber k corresponding to the bifurcation limit: single-necking mode (long wavelength limit $k \to 0$, a single diffusive neck occurs), multiple-necking mode (an intermediate wavelength $k > 0$, multiple necks appear upon the onset of bifurcation), and the surface mode (short wavelength limit $k \to \infty$, the metal surface becomes wavy). The occurrence of single-necking mode and multiple-necking mode can be retarded by attaching the metal film to an elastomer or a plastic substrate, while surface-mode limit is insensitive to the existence of a substrate. Single-necking mode occurs in a freestanding metal film or a metal film attached to a thin/compliant plastic substrate. Multiple-necking mode prevails in a metal film supported by a moderately thick/stiff plastic substrate or a thin/complaint elastomer substrate. Surface mode becomes dominating when the substrate becomes sufficiently thick or stiff.
- *Bifurcation retardation effect*: The bifurcation limit strain of a metal layer supported by an elastomer or a plastic substrate is higher than that of the counterpart freestanding metal layer, for any biaxial in-plane loading explored. The retarded bifurcation in substrate-supported metal layers essentially results from the mechanical constraint of the substrate to the metal layer deformation. (1) The bifurcation limit of an elastomer/metal bilayer depends on four parameters: the straining angle α, the hardening index of the metal film N_f, the thickness ratio H_s/H_f, and the stiffness ratio E/K. The larger H_s/H_f and E/K, the more significant necking retardation. The surface-mode limit of the metal film sets the upper bound of the retarded bifurcation limit of the elastomer/metal bilayer. (2) The bifurcation limit of a plastic/metal bilayer depends on five parameters: the straining angle α, the hardening indices of the metal film N_f and of the substrate N_s, the thickness ratio H_s/H_f, and the stiffness ratio K_s/K_f. A thicker or stiffer substrate leads to a higher bifurcation limit of an elastomer/metal bilayer. The bifurcation limit of an elastomer/metal bilayer is capped by both the surface-mode limit of the metal film and the single-necking limit of the freestanding plastic substrate.
- *Necking band orientation*: For a straining angle of $45° \leq \alpha \leq 90°$, the necking bands in substrate-supported metal layers, if occurs, are always along the direction perpendicular to that of the greater tensile strain ε_3, with $\Omega = 90°$. For a straining angle of $90° \leq \alpha \leq 116.6°$, the necking bands could appear in a slanted direction with $\Omega < 90°$. The smallest Ω occurs under uniaxial tension ($\alpha = 116.6°$). The predicted inclination angle from bifurcation analysis agrees well with the orientation of the necking bands measured in uniaxial tension experiments of substrate-supported metal layers.

We conclude by first highlighting the difference between the present study and our previous work (Jia and Li, 2013). The necking limit analysis in the previous paper is based on the assumption that occurrence of a single neck is prevailing in both freestanding metal films and substrate-supported metal films, such that a single diffusive neck is introduced accordingly as the perturbation mode. Consequently, the previous model is inadequate to precisely predict the formation of multiple necks which has been observed experimentally in substrate-supported metal films (Xiang et al., 2005). Instead of adopting a presumed single-necking mode, our current work extends the previous effort by introducing a generalized two-dimensional sinusoidal perturbation mode, through which occurrence of necking bands with any wavelength can be investigated. Prediction on bifurcation modes and bifurcation limits from the present study is more precise and realistic.

In the present analysis, the substrate-metal interface is assumed to be perfectly bonded without any interfacial delamination. In reality, interfacial debonding may occur in the substrate-metal bilayer when subjected to severe in-plane loading. With interfacial delamination, the debonded portion of the metal layer loses mechanical constraint from the substrate and thus is subject to necking formation more easily. Consequently, results presented in this theoretical work assuming perfect interfacial bonding may overestimate the bifurcation limit if interfacial debonding sets in. It is shown both numerically and experimentally that development of necking bands and interfacial delamination facilitates each other and co-evolve (Li et al., 2005; Li and Suo, 2007; Lu et al., 2007). The interfacial compliance plays a role in the deformation bifurcation of a substrate-supported metal layer (Bigoni et al., 1997). The understanding of the abovementioned effects is important but beyond the scope of this paper and we will report further studies in these regards elsewhere.

Emerging from the above findings is a structural design strategy to enhance the stretchability of metal films, that is, by well bonding a metal layer onto the surface of a substrate. We show that a moderately thick and stiff substrate can offer effective mechanical constraint to significantly increase the bifurcation limit. The results from this study can provide quantitative guidance for the material selection and structural optimization of the metal electrodes and current collectors in flexible batteries and devices. For example, we speculate that adhering lithium metal electrodes to a stretchable and

electronically-conductive substrate, such as ionic hydrogels or interpenetrating conductive polymers, may significantly enhance the performance of flexible batteries based on Li-metal technologies. We also call for further experimental studies to demonstrate design guidelines provided by the current theoretical studies.

Acknowledgments

Appendix

A1. Instantaneous moduli L_{ijkl} *for a metal layer*

The explicit form of the instantaneous moduli L_{ijkl} for a metal layer of power-law plasticity $\sigma = K\varepsilon^N$ is summarized below:

$$L_{1111} = \frac{4}{9}E_s - (E_s - E_t)\frac{1 + \sin 2\alpha}{3\left(1 + \frac{1}{2}\sin 2\alpha\right)} \tag{A1-1}$$

$$L_{2222} = \frac{4}{9}E_s - (E_s - E_t)\frac{\cos^2\alpha}{3\left(1 + \frac{1}{2}\sin 2\alpha\right)} \tag{A1-2}$$

$$L_{3333} = \frac{4}{9}E_s - (E_s - E_t)\frac{\sin^2\alpha}{3\left(1 + \frac{1}{2}\sin 2\alpha\right)} \tag{A1-3}$$

$$L_{1122} = L_{2211} = -\frac{2}{9}E_s + (E_s - E_t)\frac{\cos^2\alpha + \frac{1}{2}\sin 2\alpha}{3\left(1 + \frac{1}{2}\sin 2\alpha\right)} \tag{A1-4}$$

$$L_{1133} = L_{3311} = -\frac{2}{9}E_s + (E_s - E_t)\frac{\sin^2\alpha + \frac{1}{2}\sin 2\alpha}{3\left(1 + \frac{1}{2}\sin 2\alpha\right)} \tag{A1-5}$$

$$L_{2233} = L_{3322} = -\frac{2}{9}E_s + (E_s - E_t)\frac{\frac{1}{2}\sin 2\alpha}{3\left(1 + \frac{1}{2}\sin 2\alpha\right)} \tag{A1-6}$$

$$L_{1212} = L_{1221} = L_{2112} = L_{2121} = \frac{E_s X}{3}(-2\cos\alpha - \sin\alpha)\coth(-2X\cos\alpha - X\sin\alpha) \tag{A1-7}$$

$$L_{1313} = L_{1331} = L_{3113} = L_{3131} = \frac{E_s X}{3}(-\cos\alpha - 2\sin\alpha)\coth(-X\cos\alpha - 2X\sin\alpha) \tag{A1-8}$$

$$L_{2323} = L_{2332} = L_{3223} = L_{3232} = \frac{E_s X}{3}(\cos\alpha - \sin\alpha)\coth(X\cos\alpha - X\sin\alpha) \tag{A1-9}$$

By substituting Eqs. (8.1)–(8.2) into explicit form of L_{ijkl}, i.e. Eqs. (A1-1)–(A1-9), we have

$$L_{1111} = \left[\frac{4}{9} - (1-N)\frac{1 + \sin 2\alpha}{3\left(1 + \frac{1}{2}\sin 2\alpha\right)}\right]K\left(\frac{2}{\sqrt{3}}X\sqrt{1 + \frac{1}{2}\sin 2\alpha}\right)^{N-1} \tag{A1-10}$$

$$L_{2222} = \left[\frac{4}{9} - (1-N)\frac{\cos^2\alpha}{3\left(1 + \frac{1}{2}\sin 2\alpha\right)}\right]K\left(\frac{2}{\sqrt{3}}X\sqrt{1 + \frac{1}{2}\sin 2\alpha}\right)^{N-1} \tag{A1-11}$$

$$L_{3333} = \left[\frac{4}{9} - (1-N)\frac{\sin^2\alpha}{3\left(1+\frac{1}{2}\sin 2\alpha\right)}\right] K\left(\frac{2}{\sqrt{3}}X\sqrt{1+\frac{1}{2}\sin 2\alpha}\right)^{N-1} \tag{A1-12}$$

$$L_{1122} = L_{2211} = \left[-\frac{2}{9} + (1-N)\frac{\cos^2\alpha + \frac{1}{2}\sin 2\alpha}{3\left(1+\frac{1}{2}\sin 2\alpha\right)}\right] K\left(\frac{2}{\sqrt{3}}X\sqrt{1+\frac{1}{2}\sin 2\alpha}\right)^{N-1} \tag{A1-13}$$

$$L_{1133} = L_{3311} = \left[-\frac{2}{9} + (1-N)\frac{\sin^2\alpha + \frac{1}{2}\sin 2\alpha}{3\left(1+\frac{1}{2}\sin 2\alpha\right)}\right] K\left(\frac{2}{\sqrt{3}}X\sqrt{1+\frac{1}{2}\sin 2\alpha}\right)^{N-1} \tag{A1-14}$$

$$L_{2233} = L_{3322} = \left[-\frac{2}{9} - (1-N)\frac{\frac{1}{2}\sin 2\alpha}{3\left(1+\frac{1}{2}\sin 2\alpha\right)}\right] K\left(\frac{2}{\sqrt{3}}X\sqrt{1+\frac{1}{2}\sin 2\alpha}\right)^{N-1} \tag{A1-15}$$

$$L_{1212} = L_{1221} = L_{2112} = L_{2121} = \frac{1}{3}KX^N\left(\frac{2}{\sqrt{3}}\sqrt{1+\frac{1}{2}\sin 2\alpha}\right)^{N-1}(-2\cos\alpha - \sin\alpha)\coth(-2X\cos\alpha - X\sin\alpha) \tag{A1-16}$$

$$L_{1313} = L_{1331} = L_{3113} = L_{3131} = \frac{1}{3}KX^N\left(\frac{2}{\sqrt{3}}\sqrt{1+\frac{1}{2}\sin 2\alpha}\right)^{N-1}(-\cos\alpha - 2\sin\alpha)\coth(-X\cos\alpha - 2X\sin\alpha) \tag{A1-17}$$

$$L_{2323} = L_{2332} = L_{3223} = L_{3232} = \frac{1}{3}KX^N\left(\frac{2}{\sqrt{3}}\sqrt{1+\frac{1}{2}\sin 2\alpha}\right)^{N-1}(\cos\alpha - \sin\alpha)\coth(X\cos\alpha - X\sin\alpha) \tag{A1-18}$$

All other components of L_{ijkl} for the metal layer vanish. The components L_{ijkl} depend on X explicitly.

A2. Instantaneous moduli L_{ijkl} for an elastomer layer

All non-trivial components of instantaneous moduli L_{ijkl} of a neo-Hookean elastomer layer are explicitly summarized below

$$L_{1111} = \frac{4}{9}E\lambda_1^2 \tag{A2-1}$$

$$L_{2222} = \frac{4}{9}E\lambda_2^2 \tag{A2-2}$$

$$L_{3333} = \frac{4}{9}E\lambda_3^2 \tag{A2-3}$$

$$L_{1122} = L_{3322} = -\frac{2}{9}E\lambda_2^2 \tag{A2-4}$$

$$L_{1133} = L_{2233} = -\frac{2}{9}E\lambda_3^2 \tag{A2-5}$$

$$L_{2211} = L_{3311} = -\frac{2}{9}E\lambda_1^2 \tag{A2-6}$$

$$L_{1212} = L_{1221} = L_{2112} = L_{2121} = \frac{E}{6}\left(\lambda_1^2 + \lambda_2^2\right) \tag{A2-7}$$

$$L_{2323} = L_{2332} = L_{3223} = L_{3232} = \frac{E}{6}\left(\lambda_2^2 + \lambda_3^2\right) \tag{A2-8}$$

$$L_{1313} = L_{1331} = L_{3113} = L_{3131} = \frac{E}{6}\left(\lambda_1^2 + \lambda_3^2\right) \tag{A2-9}$$

The components L_{ijkl} for elastomer layers also depend on X explicitly.

A3. Derivation of Eq. (11) and expressions for coefficients c_{ijkl}

Any perturbation in the velocity field $v(x_1, x_2, x_3)$ induces a small increment in the asymmetric nominal stress tensor. The increment of nominal stress field is in equilibrium and the velocity field is incompressible:

$$\dot{t}_{ij,i} = 0 \tag{A3-1}$$

$$v_{i,i} = 0 \tag{A3-2}$$

where t_{ij} is the nominal stress. The relation between the Jaumann rate of Cauchy stress and the nominal stress rate is

$$\dot{t}_{ij} = \overset{\triangledown}{\sigma}_{ij} + \frac{1}{2}\sigma_{ik}v_{j,k} - \frac{1}{2}\sigma_{ik}v_{k,j} - \frac{1}{2}\sigma_{jk}v_{i,k} - \frac{1}{2}\sigma_{jk}v_{k,i} \tag{A3-3}$$

Considering the fact that σ_{ij} is homogeneous in the structure, then $\dot{t}_{ij,i} = 0$ can be rewritten as

$$c_{ijkl}v_{l,ki} + p_{,j} = 0 \ (j = 1, 3) \tag{A3-4}$$

The coefficient c_{ijkl} is given as

$$c_{ijkl} = L_{ijkl} + \frac{1}{2}\sigma_{ik}\delta_{lj} - \frac{1}{2}\sigma_{il}\delta_{kj} - \frac{1}{2}\sigma_{jk}\delta_{il} - \frac{1}{2}\sigma_{jl}\delta_{ki} \tag{A3-5}$$

Explicit expressions of c_{ijkl} for both the power-law material and the neo-Hookean elastomer are listed below

$$c_{1111} = L_{1111} - \sigma_{11} = L_{1111} \tag{A3-6}$$

$$c_{1122} = L_{1122} \tag{A3-7}$$

$$c_{1133} = L_{1133} \tag{A3-8}$$

$$c_{2112} = L_{2112} - \frac{1}{2}(\sigma_{22} + \sigma_{11}) \tag{A3-9}$$

$$c_{2121} = L_{2121} + \frac{1}{2}(\sigma_{22} - \sigma_{11}) \tag{A3-10}$$

$$c_{3113} = L_{3113} - \frac{1}{2}(\sigma_{33} + \sigma_{11}) \tag{A3-11}$$

$$c_{3131} = L_{3131} + \frac{1}{2}(\sigma_{33} - \sigma_{11}) \tag{A3-12}$$

$$c_{1212} = L_{1212} + \frac{1}{2}(\sigma_{11} - \sigma_{22}) \tag{A3-13}$$

$$c_{1221} = L_{1221} - \frac{1}{2}(\sigma_{11} + \sigma_{22}) \tag{A3-14}$$

$$c_{2211} = L_{2211} \tag{A3-15}$$

$$c_{2233} = L_{2233} \tag{A3-16}$$

$$c_{2222} = L_{2222} - \sigma_{22} \tag{A3-17}$$

$$c_{3232} = L_{3232} + \frac{1}{2}(\sigma_{33} - \sigma_{22}) \tag{A3-18}$$

$$c_{3223} = L_{3223} - \frac{1}{2}(\sigma_{33} + \sigma_{22}) \tag{A3-19}$$

$$c_{1313} = L_{1313} + \frac{1}{2}(\sigma_{11} - \sigma_{33}) \tag{A3-20}$$

$$c_{1331} = L_{1331} - \frac{1}{2}(\sigma_{11} + \sigma_{33}) \tag{A3-21}$$

$$c_{2323} = L_{2323} + \frac{1}{2}(\sigma_{22} - \sigma_{33}) \tag{A3-22}$$

$$c_{2332} = L_{2332} - \frac{1}{2}(\sigma_{22} + \sigma_{33}) \tag{A3-23}$$

$$c_{3311} = L_{3311} \tag{A3-24}$$

$$c_{3322} = L_{3322} \tag{A3-25}$$

$$c_{3333} = L_{3333} - \sigma_{33} \tag{A3-26}$$

The above expressions for c_{ijkl} hold for both the metal and elastomer layers. Also note that the coefficient c_{ijkl} depends only on the straining history X.

A4. Expressions of M_{ij}

Components of the Matrix $\boldsymbol{M}$ are given below

$$M_{11} = k^2\left(c_{1111}z^2 - c_{2121}\cos^2\Omega - c_{3131}\sin^2\Omega\right) \tag{A4-1}$$

$$M_{12} = -M_{21} = zk^2\cos\Omega(c_{1122} + c_{2112}) \tag{A4-2}$$

$$M_{13} = -M_{31} = zk^2\sin\Omega(c_{1133} + c_{3113}) \tag{A4-3}$$

$$M_{14} = M_{41} = zk \tag{A4-4}$$

$$M_{22} = k^2\left(c_{1212}z^2 - c_{2222}\cos^2\Omega - c_{3232}\sin^2\Omega\right) \tag{A4-5}$$

$$M_{23} = -M_{32} = -k^2\cos\Omega\sin\Omega(c_{2233} + c_{3223}) \tag{A4-6}$$

$$M_{24} = -M_{42} = -k\cos\Omega \tag{A4-7}$$

$$M_{33} = k^2\left(c_{1313}z^2 - c_{2323}\cos^2\Omega - c_{3333}\sin^2\Omega\right) \tag{A4-8}$$

$$M_{34} = -M_{43} = -k\sin\Omega \tag{A4-9}$$

$$M_{44} = 0 \tag{A4-10}$$

A5. C_{ji} *(i, j = 1, 6) for a freestanding metal film of thickness* h

Without losing generality, we set $x_1 = 0$ at the top surface and $x_1 = -h$ at the bottom surface of the freestanding metal film.

$$C_{1i} = c_{1111}Re\left[z_ikA_{1(i)}\right] + c_{1122}Re\left[kA_{2(i)}\right]\cos\Omega + c_{1133}Re\left[kA_{3(i)}\right]\sin\Omega + Re\left[A_{4(i)}\right] \tag{A5-1}$$

$$C_{2i} = -c_{1221}Re\left[kA_{1(i)}\right]\cos\Omega + c_{1212}Re\left[z_ikA_{2(i)}\right] \tag{A5-2}$$

$$C_{3i} = -c_{1331}Re\left[kA_{1(i)}\right]\sin\Omega + c_{1313}Re\left[z_ikA_{3(i)}\right] \tag{A5-3}$$

$$C_{4i} = c_{1111}Re\left[z_ikA_{1(i)}e^{-z_ikh}\right] + c_{1122}Re\left[kA_{2(i)}e^{-z_ikh}\right]\cos\Omega + c_{1133}Re\left[kA_{3(i)}e^{-z_ikh}\right]\sin\Omega + Re\left[A_{4(i)}e^{-z_ikh}\right] \tag{A5-4}$$

$$C_{5i} = -c_{1221}Re\left[kA_{1(i)}e^{-z_ikh}\right]\cos\Omega + c_{1212}Re\left[z_ikA_{2(i)}e^{-z_ikh}\right] \tag{A5-5}$$

$$C_{6i} = -c_{1331}Re\left[kA_{1(i)}e^{-z_ikh}\right]\sin\Omega + c_{1313}Re\left[z_ikA_{3(i)}e^{-z_ikh}\right] \tag{A5-6}$$

A6. C_{ji} $(i, j = 1, 3)$ *for a semi-infinite metal layer*

Without losing generality, we assume the semi-infinite metal layer sits in the half space of $x_1 \leq 0$, with $x_1 = 0$ being the top surface.

$$C_{1i} = c_{1111} Re\left[z_i k A_{1(i)}\right] + c_{1122} Re\left[k A_{2(i)}\right] \cos \Omega + c_{1133} Re\left[k A_{3(i)}\right] \sin \Omega + Re\left[A_{4(i)}\right] \tag{A6-1}$$

$$C_{2i} = -c_{1221} Re\left[k A_{1(i)}\right] \cos \Omega + c_{1212} Re\left[z_i k A_{2(i)}\right] \tag{A6-2}$$

$$C_{3i} = -c_{1331} Re\left[k A_{1(i)}\right] \sin \Omega + c_{1313} Re\left[z_i k A_{3(i)}\right] \tag{A6-3}$$

A7. H_{ij} *for a substrate/metal bilayer*

We set $x_1 = 0$ at the interface, $x_1 = -H$ at the bottom surface of the substrate and $x_1 = h$ at the top surface of the film. Note that, in the main text, the thickness of the substrate and the film is denoted by H_s and H_f, respectively. The Matrix **H** can be written as

$$\mathbf{H} = \begin{bmatrix}
H_{1,1} & H_{1,2} & H_{1,3} & H_{1,4} & H_{1,5} & H_{1,6} & 0 & 0 & 0 & 0 & 0 & 0 \\
H_{2,1} & H_{2,2} & H_{2,3} & H_{2,4} & H_{2,5} & H_{2,6} & 0 & 0 & 0 & 0 & 0 & 0 \\
H_{3,1} & H_{3,2} & H_{3,3} & H_{3,4} & H_{3,5} & H_{3,6} & 0 & 0 & 0 & 0 & 0 & 0 \\
H_{4,1} & H_{4,2} & H_{4,3} & H_{4,4} & H_{4,5} & H_{4,6} & H_{4,7} & H_{4,8} & H_{4,9} & H_{4,10} & H_{4,11} & H_{4,12} \\
H_{5,1} & H_{5,2} & H_{5,3} & H_{5,4} & H_{5,5} & H_{5,6} & H_{5,7} & H_{5,8} & H_{5,9} & H_{5,10} & H_{5,11} & H_{5,12} \\
H_{6,1} & H_{6,2} & H_{6,3} & H_{6,4} & H_{6,5} & H_{6,6} & H_{6,7} & H_{6,8} & H_{6,9} & H_{6,10} & H_{6,11} & H_{6,12} \\
H_{7,1} & H_{7,2} & H_{7,3} & H_{7,4} & H_{7,5} & H_{7,6} & H_{7,7} & H_{7,8} & H_{7,9} & H_{7,10} & H_{7,11} & H_{7,12} \\
H_{8,1} & H_{8,2} & H_{8,3} & H_{8,4} & H_{8,5} & H_{8,6} & H_{8,7} & H_{8,8} & H_{8,9} & H_{8,10} & H_{8,11} & H_{8,12} \\
H_{9,1} & H_{9,2} & H_{9,3} & H_{9,4} & H_{9,5} & H_{9,6} & H_{9,7} & H_{9,8} & H_{9,9} & H_{9,10} & H_{9,11} & H_{9,12} \\
0 & 0 & 0 & 0 & 0 & 0 & H_{10,7} & H_{10,8} & H_{10,9} & H_{10,10} & H_{10,11} & H_{10,12} \\
0 & 0 & 0 & 0 & 0 & 0 & H_{11,7} & H_{11,8} & H_{11,9} & H_{11,10} & H_{11,11} & H_{11,12} \\
0 & 0 & 0 & 0 & 0 & 0 & H_{12,7} & H_{12,8} & H_{12,9} & H_{12,10} & H_{12,11} & H_{12,12}
\end{bmatrix} \tag{A7-1}$$

$$H_{1,i} = c_{1111} Re\left[z_i k A^+_{1(i)} e^{z_i k h}\right] + c_{1122} Re\left[k A^+_{2(i)} e^{z_i k h}\right] \cos \Omega + c_{1133} Re\left[k A^+_{3(i)} e^{z_i k h}\right] \sin \Omega + Re\left[A^+_{4(i)} e^{z_i k h}\right] \ (i = 1, 6) \tag{A7-2}$$

$$H_{2,i} = -c_{1221} Re\left[k A^+_{1(i)} e^{z_i k h}\right] \cos \Omega + c_{1212} Re\left[z_i k A^+_{2(i)} e^{z_i k h}\right] (i = 1, 6) \tag{A7-3}$$

$$H_{3,i} = -c_{1331} Re\left[k A^+_{1(i)} e^{z_i k h}\right] \sin \Omega + c_{1313} Re\left[z_i k A^+_{3(i)} e^{z_i k h}\right] (i = 1, 6) \tag{A7-4}$$

$$H_{4,i} = Re\left[A^+_{1(i)}\right] (i = 1, 6) H_{4,i} = -Re\left[A^-_{1(i-6)}\right] (i = 7, 12) \tag{A7-5}$$

$$H_{5,i} = Re\left[A^+_{2(i)}\right] (i = 1, 6) H_{5,i} = -Re\left[A^-_{2(i-6)}\right] (i = 7, 12) \tag{A7-6}$$

$$H_{6,i} = Re\left[A^+_{3(i)}\right] (i = 1, 6) H_{6,i} = -Re\left[A^-_{3(i-6)}\right] (i = 7, 12) \tag{A7-7}$$

$$H_{7,i} = c_{1111} Re\left[z_i k A^+_{1(i)}\right] + c_{1122} Re\left[k A^+_{2(i)}\right] \cos \Omega + c_{1133} Re\left[k A^+_{3(i)}\right] \sin \Omega + Re\left[A^+_{4(i)}\right] (i = 1, 6) \tag{A7-8}$$

$$H_{7,i} = -c_{1111} Re\left[z_i k A^-_{1(i-6)}\right] - c_{1122} Re\left[k A^-_{2(i-6)}\right] \cos \Omega - c_{1133} Re\left[k A^-_{3(i-6)}\right] \sin \Omega - Re\left[A^-_{4(i-6)}\right] (i = 7, 12) \tag{A7-9}$$

$$H_{8,i} = -c_{1221} Re\left[k A^+_{1(i)}\right] \cos \Omega + c_{1212} Re\left[z_i k A^+_{2(i)}\right] (i = 1, 6) \tag{A7-10}$$

$$H_{8,i} = c_{1221} Re\left[k A^-_{1(i-6)}\right] \cos \Omega - c_{1212} Re\left[z_i k A^-_{2(i-6)}\right] (i = 7, 12) \tag{A7-11}$$

$$H_{9,i} = -c_{1331} Re\left[k A^+_{1(i)}\right] \sin \Omega + c_{1313} Re\left[z_i k A^+_{3(i)}\right] (i = 1, 6) \tag{A7-12}$$

$$H_{9,i} = c_{1331} Re\left[k A^-_{1(i-6)}\right] \sin \Omega - c_{1313} Re\left[z_i k A^-_{3(i-6)}\right] (i = 7, 12) \tag{A7-13}$$

$$H_{10,i} = c_{1111}Re\left[z_i kA^-_{1(i-6)}e^{-z_i kH}\right] + c_{1122}Re\left[kA^-_{2(i-6)}e^{-z_i kH}\right]\cos\Omega + c_{1133}Re\left[kA^-_{3(i-6)}e^{-z_i kH}\right]\sin\Omega + Re\left[A^-_{4(i-6)}e^{-z_i kH}\right](i = 7, 12)$$

(A7-14)

$$H_{11,i} = -c_{1221}Re\left[kA^-_{1(i-6)}e^{-z_i kH}\right]\cos\Omega + c_{1212}Re\left[z_i kA^-_{2(i-6)}e^{-z_i kH}\right](i = 7, 12)$$

(A7-15)

$$H_{12,i} = -c_{1331}Re\left[kA^-_{1(i-6)}e^{-z_i kH}\right]\sin\Omega + c_{1313}Re\left[z_i kA^-_{3(i-6)}e^{-z_i kH}\right](i = 7, 12)$$

(A7-16)

Reference

Alaca, B.E., Saif, M.T.A., Sehitoglu, H., 2002. On the interface debond at the edge of a thin film on a thick substrate. Acta Mater. 50, 1197–1209.

Amini, M., Nemat-Nasser, S., 2010. Micromechanisms of ductile fracturing of DH-36 steel plates under impulsive loads and influence of polyurea reinforcing. Int. J. Fract. 162, 205–217.

Amini, M.R., Isaacs, J., Nemat-Nasser, S., 2010. Investigation of effect of polyurea on response of steel plates to impulsive loads in direct pressure-pulse experiments. Mech. Mater. 42, 628–639.

Ben Bettaieb, M., Abed-Meraim, F., 2015. Investigation of localized necking in substrate-supported metal layers: comparison of bifurcation and imperfection analyses. Int. J. Plast. 65, 168–190.

Bettaieb, M.B., Abed-Meraim, F., 2017. Effect of kinematic hardening on localized necking in substrate-supported metal layers. Int. J. Mech. Sci. 123, 177–197.

Bigoni, D., Ortiz, M., Needleman, A., 1997. Effect of interfacial compliance on bifurcation of a layer bonded to a substrate. Int. J. Solids Struct. 34, 4305–4326.

Biot, M.A., 1965. Mechanics of Incremental Deformations. Wiley, New York.

Espinosa, H.D., Prorok, B.C., Fischer, M., 2003. A methodology for determining mechanical properties of freestanding thin films and MEMS materials. J. Mech. Phys. Solids 51, 47–67.

Franz, G., Abed-Meraim, F., Berveiller, M., 2013. Strain localization analysis for single crystals and polycrystals: towards microstructure-ductility linkage. Int. J. Plast. 48, 1–33.

Fu, K., Cheng, J., Li, T., Hu, L.B., 2016. Flexible batteries: from mechanics to devices. ACS Energy Lett. 1, 1065–1079.

Ghosh, A.K., 1977. Tensile instability and necking in materials with strain-hardening and strain-rate hardening. Acta Metall. 25, 1413–1424.

Gorgas, I., Herke, P., Schoeck, G., 1981. The plastic behavior of lithium single-crystals. Phys. Status Solidi A 67, 617–623.

Gruber, P., Bohm, J., Wanner, A., Sauter, L., Spolenak, R., Artz, E., 2004. Size effect on crack formation in Cu/Ta and Ta/Cu/Ta thin film systems. In: Symposium on Nanoscale Materials and Modeling held at the 2004 MRS Spring Meeting, San Francisco, CA, pp. 349–355.

Guduru, P.R., Bharath, M.S., Freund, L.B., 2006. The influence of a surface coating on the high-rate fragmentation of a ductile material. Int. J. Fract. 137, 89–108.

Guduru, P.R., Freund, L.B., 2002. The dynamics of multiple neck formation and fragmentation in high rate extension of ductile materials. Int. J. Solids Struct. 39, 5615–5632.

Haddag, B., Abed-Meraim, F., Balan, T., 2009. Strain localization analysis using a large deformation anisotropic elastic-plastic model coupled with damage. Int. J. Plast. 25, 1970–1996.

Hommel, M., Kraft, O., 2001. Deformation behavior of thin copper films on deformable substrates. Acta Mater. 49, 3935–3947.

Huang, H.B., Spaepen, F., 2000. Tensile testing of free-standing Cu, Ag and Al thin films and Ag/Cu multilayers. Acta Mater. 48, 3261–3269.

Hutchinson, J., Neale, K., 1978. Sheet necking-II. In: Time-Independent Behavior, Mechanics of Sheet Metal Forming. Springer, pp. 127–153.

Hutchinson, J.W., Tvergaard, V., 1980. Surface instabilities on statically strained plastic solids. Int. J. Mech. Sci. 22, 339–354.

Jia, Z., Li, T., 2013. Necking limit of substrate-supported metal layers under biaxial in-plane loading. Int. J. Plast. 51, 65–79.

Khan, A.S., Baig, M., 2011. Anisotropic responses, constitutive modeling and the effects of strain-rate and temperature on the formability of an aluminum alloy. Int. J. Plast. 27, 522–538.

Kim, D.H., Lu, N.S., Ma, R., Kim, Y.S., Kim, R.H., Wang, S., Wu, J., Won, S.M., Tao, H., Islam, A., Yu, K.J., Kim, T.I., Chowdhury, R., Ying, M., Xu, L., Li, M., Chung, H.J., Keum, H., McCormick, M., Liu, P., Zhang, Y.W., Omenetto, F.G., Huang, Y., Coleman, T., Rogers, J.A., 2011. Epidermal electronics. Science 333, 838–843.

Kuroda, M., Tvergaard, V., 2000. Forming limit diagrams for anisotropic metal sheets with different yield criteria. Int. J. Solids Struct. 37, 5037–5059.

Lacour, S.P., Wagner, S., Huang, Z.Y., Suo, Z., 2003. Stretchable gold conductors on elastomeric substrates. Appl. Phys. Lett. 82, 2404–2406.

Li, T., Huang, Z.Y., Xi, Z.C., Lacour, S.P., Wagner, S., Suo, Z., 2005. Delocalizing strain in a thin metal film on a polymer substrate. Mech. Mater. 37, 261–273.

Li, T., Suo, Z., 2006. Deformability of thin metal films on elastomer substrates. Int. J. Solids Struct. 43, 2351–2363.

Li, T., Suo, Z., 2007. Ductility of thin metal films on polymer substrates modulated by interfacial adhesion. Int. J. Solids Struct. 44, 1696–1705.

Liu, K., Kong, B., Liu, W., Sun, Y., Song, M.-S., Chen, J., Liu, Y., Lin, D., Pei, A., Cui, Y., 2018. Stretchable lithium metal anode with improved mechanical and electrochemical cycling stability. Joule 2, 1857–1865.

Liu, W., Song, M.S., Kong, B., Cui, Y., 2017. Flexible and stretchable energy storage: recent advances and future perspectives. Adv. Mater. 29.

Lu, N., Wang, X., Suo, Z., Vlassak, J., 2007. Metal films on polymer substrates stretched beyond 50%. Appl. Phys. Lett. 91.

Lu, N.S., Suo, Z.G., Vlassak, J.J., 2010. The effect of film thickness on the failure strain of polymer-supported metal films. Acta Mater. 58, 1679–1687.

Mansouri, L.Z., Chalal, H., Abed-Meraim, F., 2014. Ductility limit prediction using a GTN damage model coupled with localization bifurcation analysis. Mech. Mater. 76, 64–92.

Morales, S.A., Albrecht, A.B., Zhang, H., Liechti, K.M., Ravi-Chandar, K., 2011. On the dynamics of localization and fragmentation: V. Response of polymer coated Al 6061-O tubes. Int. J. Fract. 172, 161–185.

Nicola, L., Xiang, Y., Vlassak, J.J., Van der Giessen, E., Needleman, A., 2006. Plastic deformation of freestanding thin films: experiments and modeling. J. Mech. Phys. Solids 54, 2089–2110.

Shenoy, V.B., Freund, L.B., 1999. Necking bifurcations during high strain rate extension. J. Mech. Phys. Solids 47, 2209–2233.

Son, D., Lee, J., Qiao, S., Ghaffari, R., Kim, J., Lee, J.E., Song, C., Kim, S.J., Lee, D.J., Jun, S.W., Yang, S., Park, M., Shin, J., Do, K., Lee, M., Kang, K., Hwang, C.S., Lu, N., Hyeon, T., Kim, D.-H., 2014. Multifunctional wearable devices for diagnosis and therapy of movement disorders. Nat. Nanotechnol. 9, 397–404.

Song, Y.M., Xie, Y.Z., Malyarchuk, V., Xiao, J.L., Jung, I., Choi, K.J., Liu, Z.J., Park, H., Lu, C.F., Kim, R.H., Li, R., Crozier, K.B., Huang, Y.G., Rogers, J.A., 2013. Digital cameras with designs inspired by the arthropod eye. Nature 497, 95–99.

Storen, S., Rice, J.R., 1975. Localized necking in thin sheets. J. Mech. Phys. Solids 23, 421–441.

Tvergaard, V., 1978. Effect of kinematic hardening on localized necking in biaxially stretched sheets. Int. J. Mech. Sci. 20, 651–658.

Vandeparre, H., Liu, Q.H., Minev, I.R., Suo, Z.G., Lacour, S.P., 2013. Localization of folds and cracks in thin metal films coated on flexible elastomer foams. Adv. Mater. 25, 3117–3121.

Xiang, Y., Li, T., Suo, Z.G., Vlassak, J.J., 2005. High ductility of a metal film adherent on a polymer substrate. Appl. Phys. Lett. 87, 161910.

Xu, S., Zhang, Y.H., Cho, J., Lee, J., Huang, X., Jia, L., Fan, J.A., Su, Y.W., Su, J., Zhang, H.G., Cheng, H.Y., Lu, B.W., Yu, C.J., Chuang, C., Kim, T.I., Song, T., Shigeta, K., Kang, S., Dagdeviren, C., Petrov, I., Braun, P.V., Huang, Y.G., Paik, U., Rogers, J.A., 2013. Stretchable batteries with self-similar serpentine interconnects and integrated wireless recharging systems. Nat. Commun. 4, 1543.

Xue, Z.Y., Hutchinson, J.W., 2007. Neck retardation and enhanced energy absorption in metal-elastomer bilayers. Mech. Mater. 39, 473–487.

Xue, Z.Y., Hutchinson, J.W., 2008. Neck development in metal/elastomer bilayers under dynamic stretchings. Int. J. Solids Struct. 45, 3769–3778.

Yang, S.X., Chen, Y.C., Nicolini, L., Pasupathy, P., Sacks, J., Su, B., Yang, R., Sanchez, D., Chang, Y.F., Wang, P.L., Schnyer, D., Neikirk, D., Lu, N.S., 2015. Cut-and–paste manufacture of multiparametric epidermal sensor systems. Adv. Mater. 27, 6423 -+.

Yu, D.Y.W., Spaepen, F., 2004. The yield strength of thin copper films on Kapton. J. Appl. Phys. 95, 2991–2997.

Zhang, H., Ravi-Chandar, K., 2006. On the dynamics of necking and fragmentation - I. Real-time and post-mortem observations in Al6061-O. Int. J. Fract. 142, 183–217.

Zhang, L., Wang, J., 2012. Modeling the localized necking in anisotropic sheet metals. Int. J. Plast. 39, 103–118.

Zhang, Y.H., Huang, Y.G., Rogers, J.A., 2015. Mechanics of stretchable batteries and supercapacitors. Curr. Opin. Solid State Mater. Sci. 19, 190–199.